이학석사학위논문

Evaluation of Impacts of Grid Refinement on Behavior and Trapping Mechanisms of Carbon Dioxide Injected into Deep Storage Formations

심부 저장 지층에 주입된 이산화탄소의 거동 및 포획 기작에 대한 격자 세분할의 영향 평가

2015년 2월

서울대학교 대학원

지구환경과학부

이 성 호

Evaluation of Impacts of Grid Refinement on Behavior and Trapping Mechanisms of Carbon Dioxide Injected into Deep Storage Formations

심부 저장 지층에 주입된 이산화탄소의 거동 및 포획 기작에 대한 격자 세분할의 영향 평가

지도교수 김 준 모

이 논문을 이학석사학위논문으로 제출함
2014년 12월

서울대학교 대학원
지구환경과학부
이 성 호

이성호의 이학석사학위논문을 인준함
2014년 12월

위 원 장 이 용 일 (인)
부위원장 김 준 모 (인)
위 원 이 강 근 (인)

Abstract

Evaluation of Impacts of Grid Refinement on Behavior and Trapping Mechanisms of Carbon Dioxide Injected into Deep Storage Formations

Sungho Lee

School of Earth and Environmental Sciences

The Graduate School

Seoul National University

A series of numerical simulation using a multi-phase thermo-hydro numerical model is performed to quantitatively evaluate impacts of grid refinement in vertical direction, horizontal direction, and both directions on behavior and trapping mechanisms of injected carbon dioxide (CO_2) into deep storage formations. First of all, the modeling domain is discretized into base case. Then it is further discretized into a half, a quarter, and one-eighth in each individual direction and both directions. The results of numerical simulation show that spatial-temporal behavior (both free fluid phase and aqueous phase

CO_2) and trapping mechanisms (both hydrodynamic and solubility) of injected CO_2 are significant to grid refinement in vertical (z) direction, horizontal (xy) direction and both directions (xyz). For all these reasons, it is found that grid refinement in each individual direction and both directions can accurately consider sharp fronts of injected CO_2 but also can accurately consider both pressure and temperature in the storage formation. As a result, the relative coarse grids have smooth spacious fronts of injected CO_2 in injection period regardless of grid refinement in each individual direction and both directions. Also, they have smooth spacious fronts of injected CO_2 as well as underestimates radial extent of injected CO_2 after CO_2 injection is finished. Meanwhile, the results of numerical simulation show that injected CO_2 mainly moves in horizontal direction in CO_2 injection period, however, it moves in vertical direction after CO_2 injection is finished regardless of grid refinement. Then, grid refinement in horizontal direction mainly affects behavior and trapping mechanisms of injected CO_2 in CO_2 injection period, In contrast, grid refinement in vertical direction mainly affects behavior and trapping mechanisms of injected CO_2 after CO_2 injection is finished. Thus, grid refinement in both directions has apparently similar trends of the results of grid refinement in horizontal direction in CO_2 injection period, and similar trends of the results of grid refinement in vertical direction after CO_2 injection

is finished. It turned out that these numerical results strongly suggest that grid size both directions plays important role to accurately predict behavior and trapping mechanisms of injected CO_2 before and after CO_2 injection is finished.

Keywords: geologic carbon dioxide storage, deep storage formations, behavior mechanism, trapping mechanism, grid refinement, numerical modeling

***Student Number*: 2013-20336**

Contents

List of Tables

List of Figures

1. Introduction

Geologic carbon dioxide (CO_2) storage is has been considered as an effective countermeasure for reducing the rate of CO_2 emissions (Holloway, 1997; Metz et al., 2005). Geologic storage of CO_2 involves sequestration of CO_2 in suitable deep geologic formations such as saline aquifers, oil and gas reservoirs and coal beds. Once CO_2 is injected, it is stored through a series of trapping mechanisms and is finally sequestrated permanently in the deep subsurface, which is separated from the atmosphere (Metz et al., 2005).

In order to conduct geologic CO_2 storage, the variety of technologies are used. Among them, the six key technologies are identified by work of Metz et al. (2005) as follows: (1) site (geologic formation) characterization and evaluation technology, (2) well drilling and injection technology, (3) CO_2 behavior prediction technology, (4) CO_2 monitoring technology, (5) environment impact assessment technology, and (6) management and utilization technology for closed sites. Among them, these (3), (4), (5), and (6) are also divided into monitoring, mitigation, and verification (MMV) or monitoring, verification, and accounting (MVA) technologies (Metz et al., 2005; Litynski et al., 2012). Recently, these MMV and MVA technologies become important because the concept of possible measurements, reporting and verification as reduction measures of CO_2 emission appeared in the Bali

Road Map.

CO_2 behavior prediction (numerical modeling) technology to analyze flow mechanisms of injected CO_2 into a target basin or a target formation, and to evaluate trapping and leakage mechanisms of CO_2 by using multi-phase thermo-hydro-mechanical-chemical (T-H-M-C) numerical modeling. CO_2 behavior (flow, trapping, leakage mechanisms) prediction technology can play a most central role in the overall implementation for integrated numerical modeling of CO_2 geological storage technology because it is directly utilized in conjunction with evaluation of target geologic formation system (reservoir rock + cap rock + groundwater) performance (injection capacity, storage capacity, seal capacity) and risk analysis of CO_2 leakage through abandoned wells or faults. Three-dimensional geologic modeling or other modeling technologies are also integrated with CO_2 behavior prediction technology. Therefore, it is essential to take advantage of this CO_2 behavior prediction technology for successful CO_2 geological storage projects. From outside, CMG-GHG (Computer Modeling Group, 2009), STOMP (White and Oostrom, 2006), TOUGH2 (Pruess et al., 1999) and various behavior prediction numerical models have been used to predict behavior and trapping mechanisms of CO_2 and analyze the variety of phenomena according to injected CO_2 into target formation (e.g., Rutqvist et al., 2002; Johnson et al.,

2004; White et al., 2005; Zhang et al; Lindeberg et al., 2009; Scottish Carbon Capture and Storage, 2011; Smith et al., 2011; Xu et al., 2011). From inside, CO_2 behavior prediction models are actively used to analyze behavior mechanisms and evaluate trapping mechanisms. Firstly, a series of thermo-hydro numerical modeling was performed to investigate multi-phase fluid flow and heat transport associated with CO_2 geologic storage (Kihm and Kim, 2007; Kim, 2008; Kim, 2009). A series of thermo-hydro-mechanical modeling was then performed to integratedly investigate multi-phase fluid flow, heat transport and mechanical deformation (Kihm and Kim, 2008; Park et al., 2011). Furthermore, a series of thermo-hydro-chemical modeling was performed to analyze multi-phase fluid flow, heat transport and hydrogeochemical reactive solute transport and then comprehensively evaluate trapping mechanisms (Kihm et al., 2012a; Kihm et al., 2012b). These studies had been conducted to analyze coupled thermo-hydro-mechanical-chemical phenomena and evaluate applicability in a relatively simplified formation since these CO_2 behavior prediction technologies were first introduced. In other words, these were conducted to obtain behavior prediction technology among the six key technologies for geologic CO_2 storage.

Meanwhile, insufficient spatial resolution is commonly recognized to be

the primary source of errors in numerical solutions of partial differential equations (PDEs) for water flow and solute (mass) transport in the vadose zone (Yeh, 2000). Critical problems related grid resolution are such as penetration of sharp wetting fronts during infiltration in initially dry soil due to highly non-linear relationships between hydraulic conductivity and pressure head or sharp concentration fronts during convection-dominant solute transport (Mansell et al., 2002). Conceptually, it is similar that water body (Sw $\approx$ 1) infiltrates suddenly into initially dry soil (Sg $\approx$ 1) and conversely CO_2 (Sg $\approx$ 1) is injected suddenly into deep saline aquifer (Sw $\approx$ 1). In other words, numerical predictions for geologic storage of CO_2 into deep saline aquifer also can be a critical case requiring grid refinement. In addition, thermophysical properties of CO_2 are density and viscosity (Fig. 1) (Spycher and Pruess, 2005). They are dependent on pressure, temperature and mass fraction and they has strong non-linearity, because CO_2 has large compressibility in comparison with groundwater (Fig. 2). Thus, CO_2 density and viscosity are very significant to spatial discretization of numerical modeling domain, because of their non-linear characteristic (Fig. 3). Consequently, behavior of CO_2 is also significant to spatial discretization of numerical modeling domain, because a multi-phase fluid flow governing equation includes relative permeability, density and viscosity as constitutive

terms, which for an individual fluid phase α can be expressed as follows:

$$q_\alpha = k\frac{k_{r\alpha}}{\mu_\alpha}\rho_\alpha(\nabla p + \rho_\alpha g \nabla z) \quad (1)$$

, where q_α is mass flux, k is intrinsic permeability, $k_{r\alpha}$ is relative permeability μ_α is fluid viscosity, ρ_α is fluid density, p is pressure head g is gravitational acceleration, and z is elevation head. From outside, grid size and grid shape were investigated by few studies because of above-mentioned reason (e.g. Doughty and Pruess, 2004; Yamamoto and Doughty, 2011). First of all, Doughty and Pruess (2004) investigated impacts of grid refinement in vertical direction and heterogeneity which targets for fluvial deltaic Frio formation in the upper gulf coast, Texas. Since then, Yamamoto and Doughty (2011) investigated impacts of grid refinement in vertical direction and grid shape which targets for Vedder formation subsurface the southern San Joaquin Valley, California. These previous studies strongly suggest that coarse grid of numerical modeling domain in vertical direction underestimates maximum radial extent of injected CO_2 plume. However, the work of Doughty and Pruess (2004) show behavior of CO_2 is large affected by boundary condition because of relative small numerical domain size in comparison to CO_2 injection amount. Even though injected CO_2 flows in both

vertical and horizontal direction, these studies only evaluate grid refinement in vertical direction as well. From inside, on the other hand, impacts of grid size and grid shape on behavior and trapping mechanisms of injected CO_2 have not been evaluated yet. However, Kim (2014) performed a series of thermo-hydrological numerical modeling to predict and analyze behavior of carbon dioxide injected into target geologic formations in the Gyeongsang Basin, Korea. The results point out that hydrodynamic trapping does not occur in basin scale for small amount injection, because all injected CO_2 is immediately stored by solubility trapping. Thus, it is necessary that evaluation of impacts of grid refinement on behavior and trapping mechanisms of CO_2 in both directions and determination of proper grid size in both directions for scale of injection amount and storage site. Beforehand evaluation of grid refinement to real storage site, grid refinement in both directions including individuals preliminarily must be conducted in a hypothetical geologic CO_2 storage formation.

The objectives of this study are to quantitatively analyze and evaluate impacts of grid refinement on behavior and trapping of large amount of CO_2 (more than 1 Mton/year) injected into the storage formation. In order to achieve these objectives, the storage formation was first discretized into regular grid size (base case,). It was then further discretized into a half, a

quarter, and one-eighth in each individual direction, and both vertical and horizontal directions. Then, a series of multi-phase thermo-hydro numerical modeling was performed.

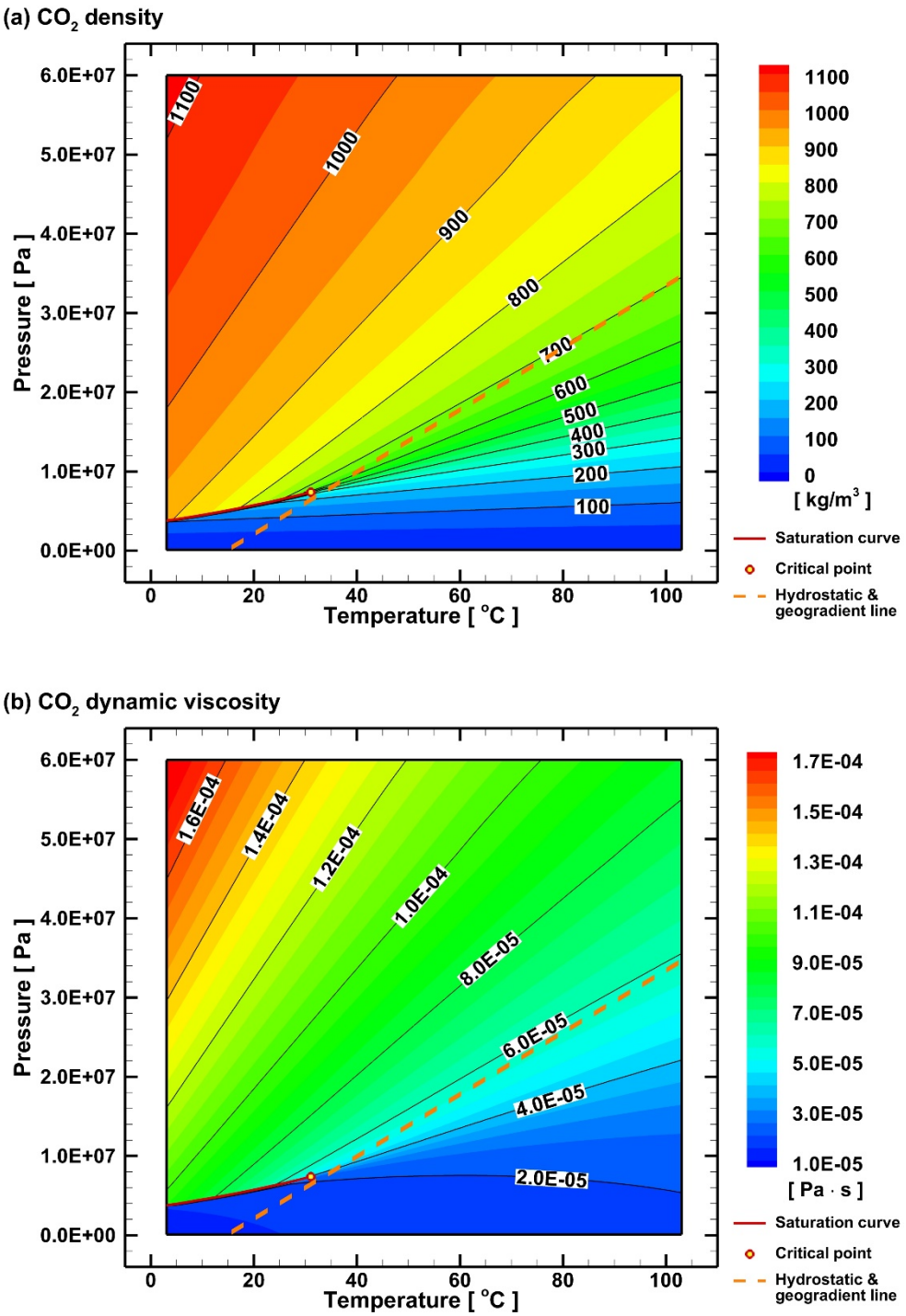

Figure 1. Diagram of CO_2 (a) density and (b) viscosity.

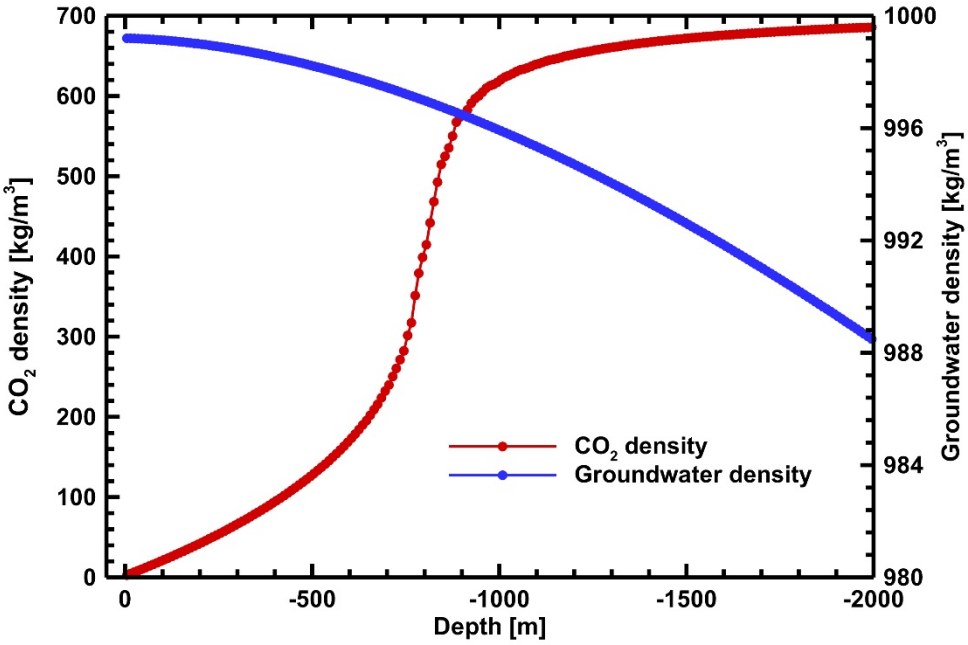

Figure 2. Diagram of density of CO_2 and groundwater profile with depth.

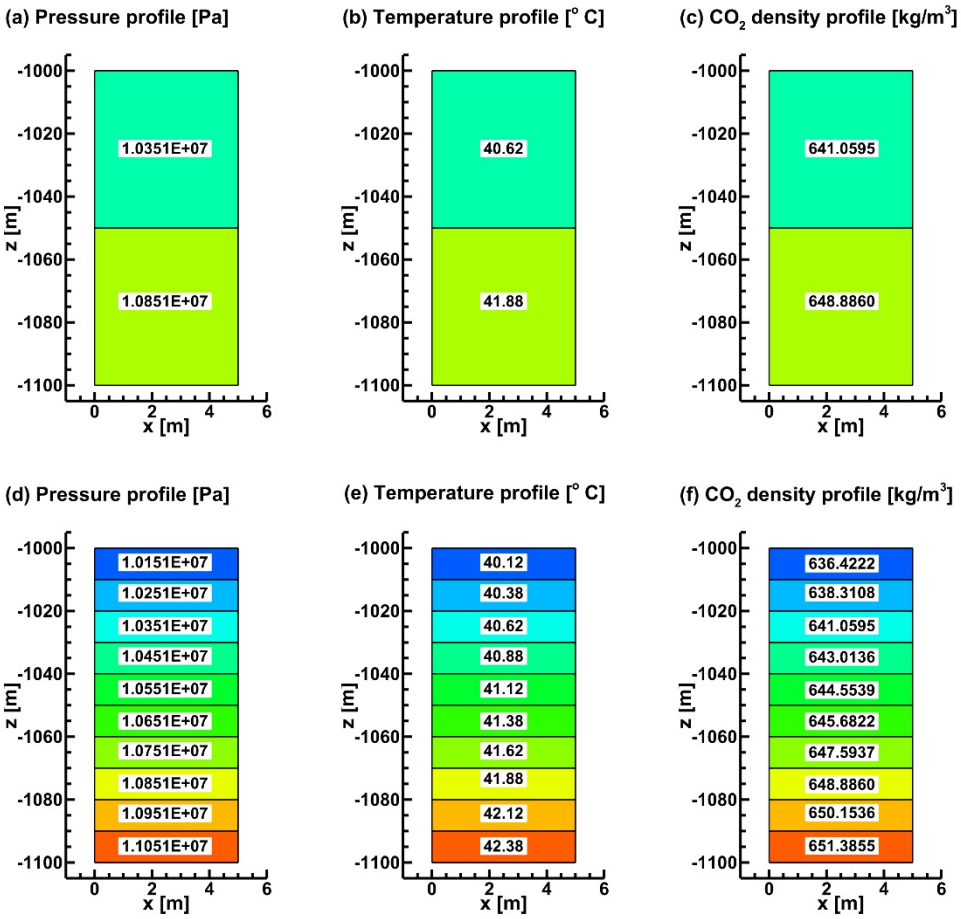

Figure 3. Diagram of pressure profile with depth in (a) coarse grid and in (d) fine grid. Diagram of temperature profile with depth in (b) coarse grid and in (e) fine grid. Diagram of CO_2 density profile with depth in (c) coarse grid and in (f) fine grid.

2. Numerical model

The multi-phase fluid flow and heat transport numerical model TOUGH2-MP (Zhang et al., 2008) is used in this study. TOUGH2-MP was developed by parallelizing the multi-phase fluid flow and heat transport numerical model TOUGH2 based on message passing interface (MPI). TOUGH2-MP is based on spatial discretization by means of an integral finite difference (IFD) method which provides flexible spatial discretization for geologic media by allowing the use of irregular grid blocks (Narasimhan and Witherspoon, 1976). TOUGH2-MP includes also one of kind of domain decomposition METIS (Karypsis, 2013) software which divides a numerical modeling domain into several sub-domain (Fig. 4) (Zhang et al., 2008). Thus, TOUGH2-MP is suitable to simulate flow and transport in large scale heterogeneous and fractured rock systems with various and heterogeneous petrology. In TOUGH2-MP, properties of fluid or fluid mixture with aqueous components are considered by various EOS (equation of state) modules. A fluid property EOS module ECO2N based on the work of Spycher and Pruess (2005) is used in this study. The ECO2N module provides an accurate description of the thermophysical properties of mixture of water and CO_2 under conditions typically encountered in saline aquifers of interest for geologic storage of CO_2 (i.e., $10^oC \leq T \leq 110^oC$, $P \leq 100$ bars).

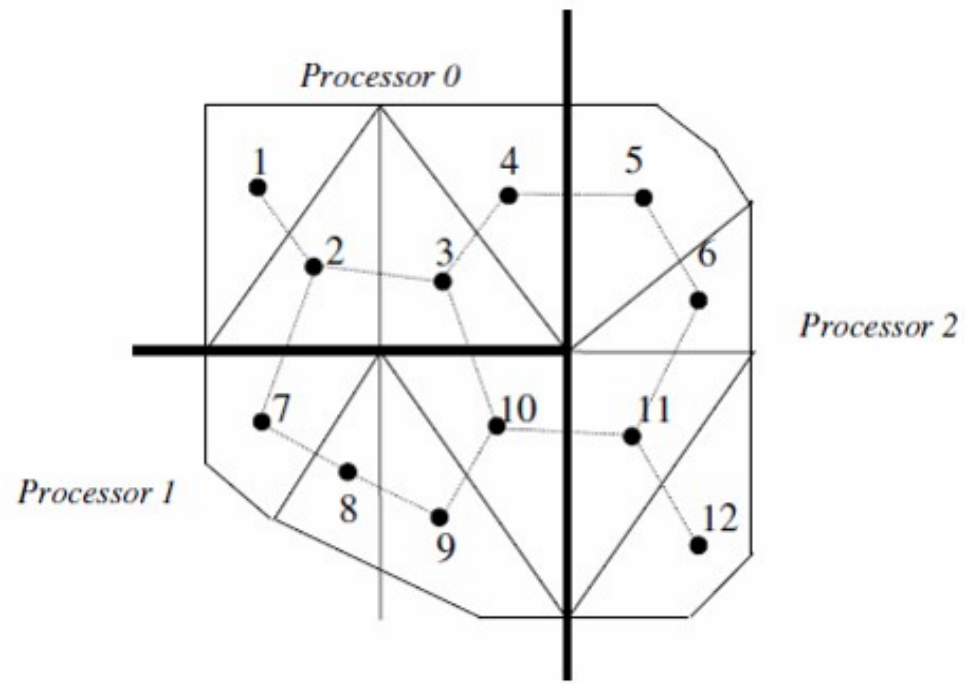

Figure 4. Schematic diagram of domain decomposition into sub-domain (Zhang et al., 2008)

3. Numerical simulations

Hosa et al. (2011) examined current or completed worldwide 20 CO_2 injection projects in saline formation aquifer and classified those characteristics. According to the study, large scale or commercial scale (over than annually 1 Mton) projects are summarized such as Sleipner and Snøhvit in Norway, Gorgon in Australia, In Salah in Algeria, and Weyburn in Canada. The study shows that those large scale projects are between 800 m ~ 2,500 m deep and between 29 m ~ 500 m thickness of saline aquifer. Thus, a hypothetical modeling domain is constructed to consider geological depth and aquifer thickness of current large scale projects in this study. A above-mentioned the hypothetical sandstone formation (reservoir rock) is conceptualized as a three-dimensional modeling domain with thickness of 100 m and extent of 6,000 m, and it is located at depths between 1,500 m (z = 100 m) and 1,600 m (z = 0 m) from ground surface (Fig. 5). It is assumed to be underlain and overlain by two impermeable shale layers (upper cap rock and lower bedrock). The modeling domain is then discretized into 4,805 grid blocks as the base case (Case 1). Then it is further discretized into a half, a quarter, and one-eighth in vertical (z), horizontal (xy) and both (xyz) directions (Fig. 6). Consequentially, all cases are more fine than the base case (case 1) and the most fine case (Case xyz-8) discretized into one-eighth in

both direction has 2,460,160 grid blocks. On the other hand, injection well is fixed to 0.25 m radius over all cases. The cases of this study are listed on Table 1.

The initial condition of fluid pressure for those cases is applied such that it increases hydrostatically with depth to consider no-flow condition at the beginning. The initial condition of temperature increase with 0.025 ^{o}C/m geothermal gradient, here atmospheric temperature is assumed to be 15 ^{o}C at ground surface. Initial salinity is set to 35,000 ppm for entire modeling domain. Along the top and bottom boundaries, no-flow and no-transport, are assigned considering the impermeable shale layers for cap rock and bed rock. Along the out boundaries, the Dirichlet-type flow and transport boundary conditions which are equivalent to initial condition are assigned considering the infinite extent of the modeling domain.

CO_2 is injected through the screen interval of 20 m at the bottom of the CO_2 injection well at a constant rate of 31.71 kg/sec (1 Mton/year) for 1 year. The total simulation time period is set equal to 200 year including the CO_2 injection period of 1 year. The hydrogeological properties of the sandstone aquifer are assumed to be homogeneous and isotropic. Hydrogeological properties from the work of Xu et al (2012) are used in this study and they are listed in Table 2.

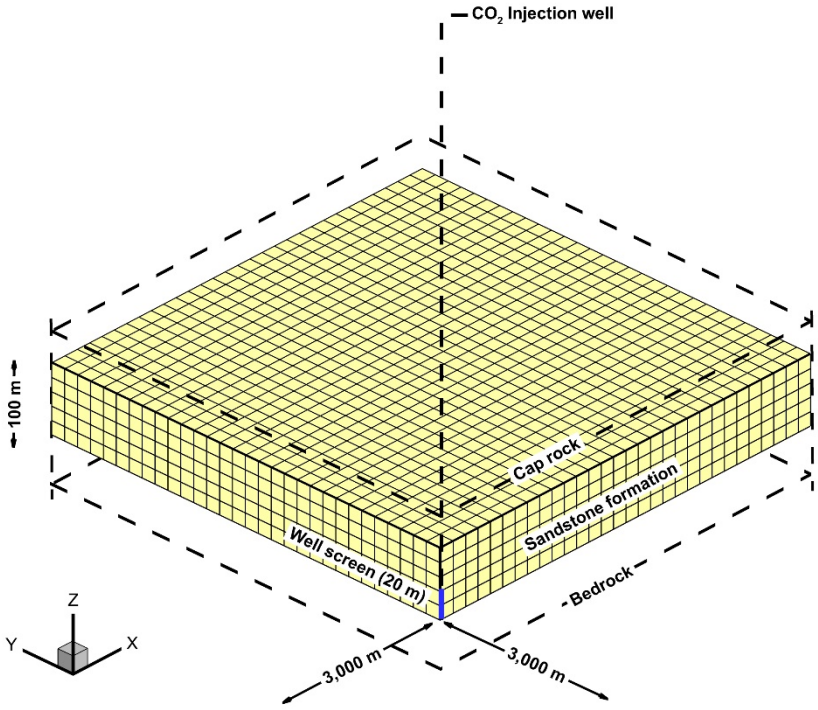

Figure 5. Schematic diagram of the hypothetical sandstone aquifer modeling domain) and CO_2 injection well used in the numerical simulation.

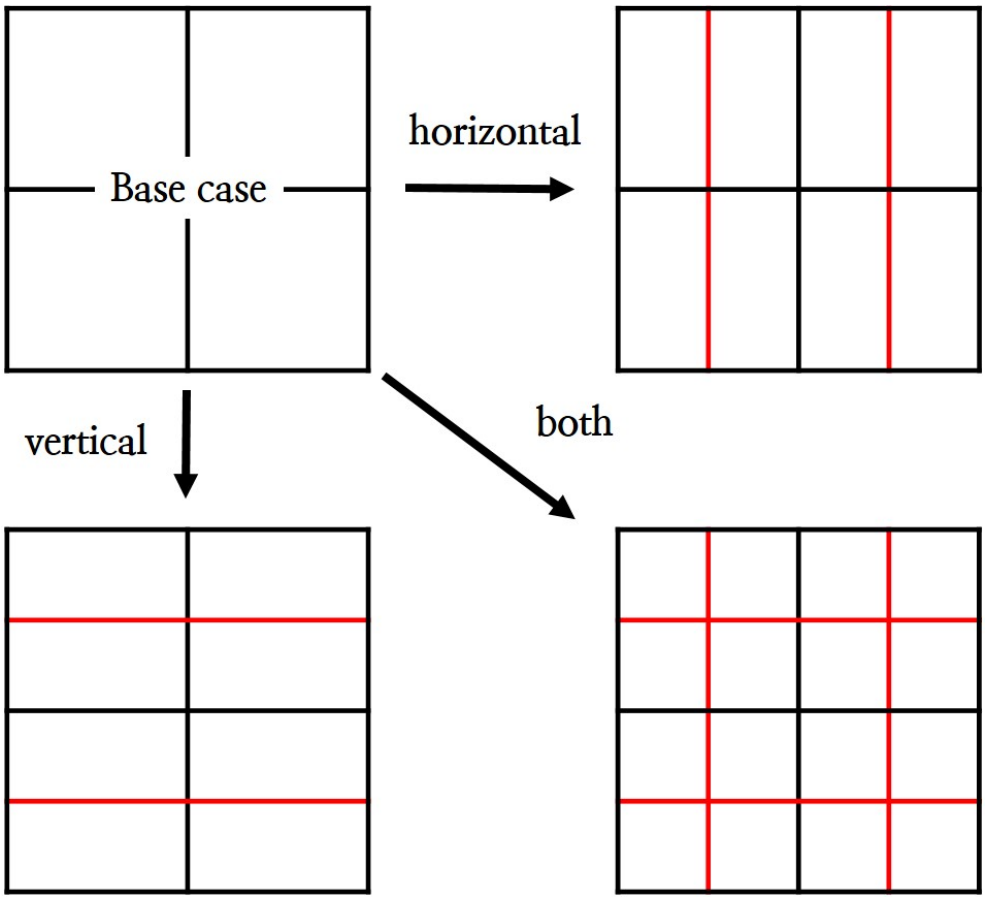

Figure 6. Schematic diagram for grid refinement in each individual direction and both directions.

Table 2. The cases description with grid refinement in individual and both direction.

	Direction	Case	Grid refinement	Number of grid blocks
Base case (Case 1) (4,805 grids)	z (vertical)	Case z-2	1/2	9,610
		Case z-4	1/4	19,220
		Case z-8	1/8	38,400
	xy (horizontal)	Case xy-2	1/2	19,200
		Case xy-4	1/4	76,800
		Case xy-8	1/8	307,520
	xyz (both)	Case xyz-2	1/2	38,400
		Case xyz-4	1/4	307,520
		Case xyz-8	1/8	2,460,160

Table 2. Hydrogeological properties of the storage formation (sandstone) (Xu et al., 2012).

Property	Value
Porosity	0.30
Intrinsic permeability [m^2]	1.00×10^{-13}
Compressibility [Pa^{-1}]	4.51×10^{-10}
Relative permeability of liquid (van Genuchten, 1980)	
$k_{rl} = \sqrt{S^*}\{1 - [1 - (S^*)^{1/m}]^m\}^2$ where $S^* = (S_l - S_{lr})/(1 - S_{lr})$	
Residual liquid saturation S_{lr}	0.30
Exponent m	0.457
Relative permeability of gas (Corey, 1954)	
$k_{rg} = (1 - \hat{S})^2(1 - \hat{S}^2)$ where $\hat{S} = (S_l - S_{lr})/(1 - S_{lr} - S_{gr})$	
Residual gas saturation S_{gr}	0.05
Capillary pressure (van Genuchten, 1980)	
$P_c = -P_0[(S^*)^{-1/m} - 1]^{1-m}$ where $S^* = (S_l - S_{lr})/(1 - S_{lr})$	
Residual liquid saturation S_{lr}	0.00
Exponent m	0.457
Strength coefficient (gas entry pressure) P_0 [Pa]	1.961×10^4

4. Results and analyses

4.1. Saturation of free fluid phase CO_2

The spatial distributions of saturation of free fluid phase CO_2 in the storage formation for Case z including base case after 10 days, 1 year, 5 years, and 200 years in Fig. 7, Fig. 8, Fig. 9, and Fig. 10 respectively. In CO_2 injection period, injected CO_2 initially moves upward due to pressure gradient and buoyancy force (density difference between CO_2 and groundwater) and then saturation of free fluid phase CO_2 is reached to cap rock overall all cases at the end of CO_2 injection (Fig. 7 and Fig. 8). However, spatial distributions have difference with grid refinement in vertical direction (Fig. 7a, 7b, 7c, 7d and Fig. 8a, 8b, 8c, 8d). Saturation of free fluid phase CO_2 less moves upward at the beginning of CO_2 injection (10 days) and then evidently becomes less underneath cap rock and above bed rock at the end of CO_2 injection (1 year) with grid refinement in vertical direction (Fig. 7a, 7b, 7c, 7d and Fig. 8a, 8b, 8c, 8d). As a result, plume (saturation group) of free fluid phase CO_2 is changed from bell-shaped to gourd-shaped at the end of CO_2 injection with grid refinement in vertical direction (Fig. 8a, 8b, 8c, 8d). After CO_2 injection is completely finished, CO_2 mostly moves upward and then laterally along cap rock due to buoyancy force (Fig. 9). Consequently, saturation of free fluid

phase CO_2 then mostly remains underneath cap rock (Fig. 10). However, spatial distributions have also difference with grid refinement in vertical direction (Fig. 9a, 9b, 9c, 9d and Fig. 10a, 10b, 10c, 10d). Plume of free fluid phase CO_2 obviously becomes thin in vertical direction and moves far laterally along cap rock with grid refinement in vertical direction (Fig. 9a, 9b, 9c, 9d and Fig. 10a, 10b, 10c, 10d). As a result, radius of free phase CO_2 influence increases at the end of simulation with grid refinement in vertical direction (Fig. 10a, 10b, 10c, 10d).

The spatial distributions of saturation of free fluid phase CO_2 in the storage formation for Case xy including base case after 10 days, 1 year, 5 years, and 200 years in Fig. 11, Fig. 12, Fig. 13, and Fig. 14 respectively. In CO_2 injection period, injected CO_2 initially moves upward and then saturation of free fluid phase CO_2 is reached to cap rock overall all cases at the end of CO_2 injection (Fig. 11 and Fig. 12). However, spatial distributions have difference with grid refinement in horizontal direction (Fig. 11a, 11b, 11c, 11d and Fig. 12a, 12b, 12c, 12d). Saturation of free fluid phase CO_2 less moves laterally at the beginning of CO_2 injection and then is entirely distributed in horizontally narrow space as well as increases around the screen of injection well at the end of CO_2 injection with grid refinement in horizontal direction (Fig. 11a, 11b, 11c, 11d and Fig. 12a, 12b, 12c, 12d). As a result, plume of

free fluid phase CO_2 is changed from bell-shaped to upside down pyramid-shaped at the end of CO_2 injection with grid refinement in horizontal direction (Fig. 12a, 12b, 12c, 12d). After CO_2 injection is completely finished, spatial distributions have also difference with grid refinement in horizontal direction (Fig. 13a, 13b, 13c, 13d and Fig. 14a, 14b, 14c, 14d). Saturation of free fluid phase CO_2 obviously tends to increase near the injection well and underneath cap rock with grid refinement in horizontal direction (Fig. 13a, 13b, 13c, 13d and Fig. 14a, 14b, 14c, 14d). As a result, radius of free phase CO_2 influence increases at the end of simulation with grid refinement in horizontal direction (Fig. 14a, 14b, 14c, 14d).

The spatial distributions of saturation of free fluid phase CO_2 in the storage formation for Case xyz including base case after 10 days, 1 year, 5 years, and 200 years in Fig. 15, Fig. 16, Fig. 17, and Fig. 18 respectively. In CO_2 injection period, injected CO_2 initially moves upward and then saturation of free fluid phase CO_2 is reached to cap rock overall all cases at the end of CO_2 injection (Fig. 15 and Fig. 16). However, spatial distributions have difference with grid refinement in both directions (Fig. 15a, 15b, 15c, 15d and Fig. 16a, 16b, 16c, 16d). Saturation of free fluid phase CO_2 less moves in both directions at the beginning of CO_2 injection and then is entirely distributed in horizontally narrow space as well as increases around the screen of injection

well at the end of CO_2 injection with grid refinement in both directions (Fig. 15a, 15b, 15c, 15d and Fig. 16a, 16b, 16c, 16d). As a result, , plume of free fluid phase CO_2 is changed from bell-shaped to upside down gourd-shaped at the end of CO_2 injection with grid refinement in both directions (Fig. 16a, 16b, 16c, 16d). After CO_2 injection is completely finished, spatial distributions have also difference with grid refinement in both directions (Fig. 17a, 17b, 17c, 17d and Fig. 18a, 18b, 18c, 18d). Saturation of free fluid phase CO_2 obviously tends to increase underneath cap rock and moves far laterally along cap rock with grid refinement in both directions (Fig. 17a, 17b, 17c, 17d and Fig. 18a, 18b, 18c, 18d). As a result, radius of free phase CO_2 influence increases at the end of simulation with grid refinement in both directions (Fig. 18a, 18b, 18c, 18d).

As mentioned above, CO_2 injection into storage formations including no initial CO_2 is similar to water body or NAPLs infiltration into initial dry soil. In addition, CO_2 has large compressibility with depth (Fig. 2). In other words, the above-mentioned numerical simulation results are interpreted as grid refinement is supposed to accurately consider sharp front of injected CO_2 and both pressure and temperature in the storage formation. Firstly, grid refinement in vertical direction can consider sharp front in vertical direction and lower pressure and temperature (i.e., lower CO_2 density) underneath cap

rock and higher pressure and temperature (i.e., higher CO_2 density) above bed rock than that of no grid refinement (Fig 3c, 3f). Consequently, saturation of free fluid phase CO_2 become sharp front in vertical direction (along injection well) and buoyancy force gradually increases as CO_2 moves upward, and then plume of free phase CO_2 can fast moves upward as CO_2 closes to cap rock and moves far along cap rock. Secondly, grid refinement in horizontal direction can consider sharp front in horizontal direction than that of no grid refinement. As a result, saturation of free fluid phase CO_2 become sharp front in horizontal direction, and then saturation of free fluid phase CO_2 presents in narrow space, increases around the screen of injection well, and consequently increases underneath cap rock in the logical order. Finally, grid refinement in both directions can consider sharp front in both directions and both pressure and temperature in the storage formation, thus it includes impacts of grid refinement in each individual direction. However, behavior of free fluid phase CO_2 with grid refinement in both directions is obviously similar to behavior of free phase CO_2 with grid refinement in horizontal direction in CO_2 injection period, whereas behavior of free fluid phase CO_2 with grid refinement in both directions is obviously similar to behavior of free phase CO_2 with grid refinement in vertical direction after CO_2 injection is finished. In other words, free fluid phase CO_2 is sensitive to grid in horizontal

direction during CO_2 injection, on the other hand, free fluid phase CO_2 is sensitive to grid in vertical direction after CO_2 injection is finished.

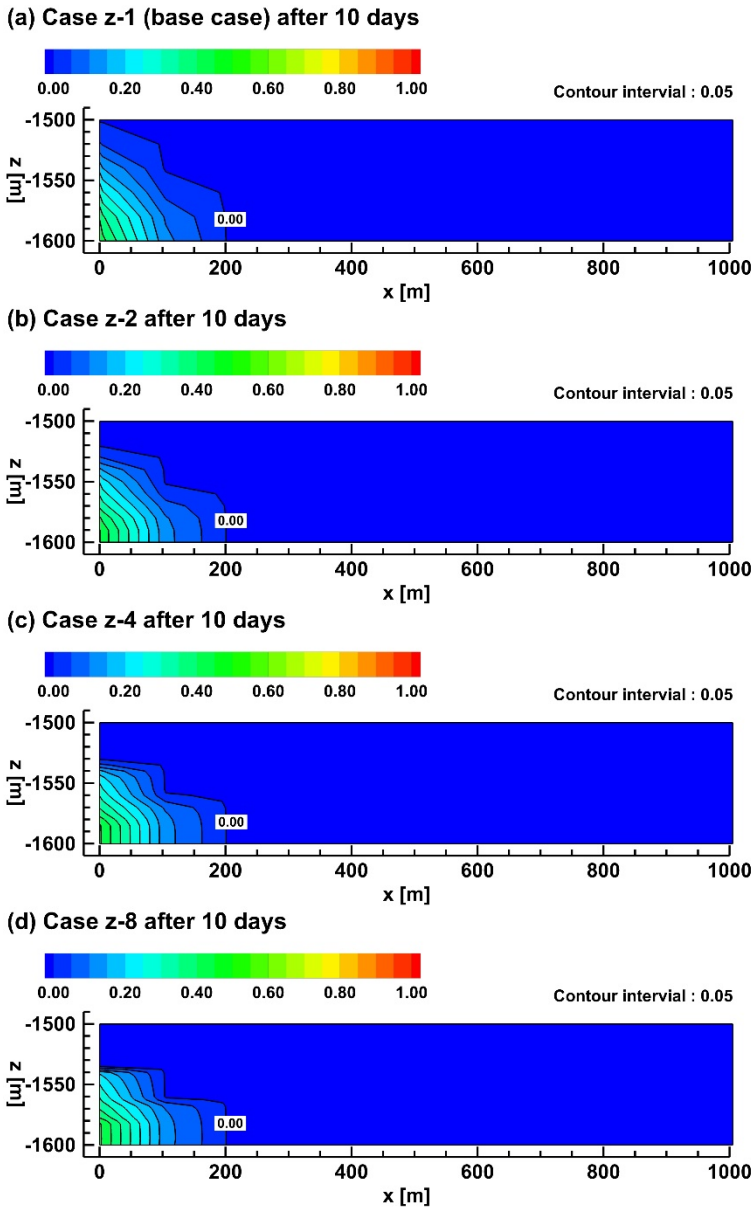

Figure 7. Spatial distributions of saturation of free fluid phase CO_2 in the storage formation after 10 days for (a) base case, (b) Case z-2, (c) Case z-4, (d) Case z-8 since the start of CO_2 injection. Note that this figure is cross section view (y = 0).

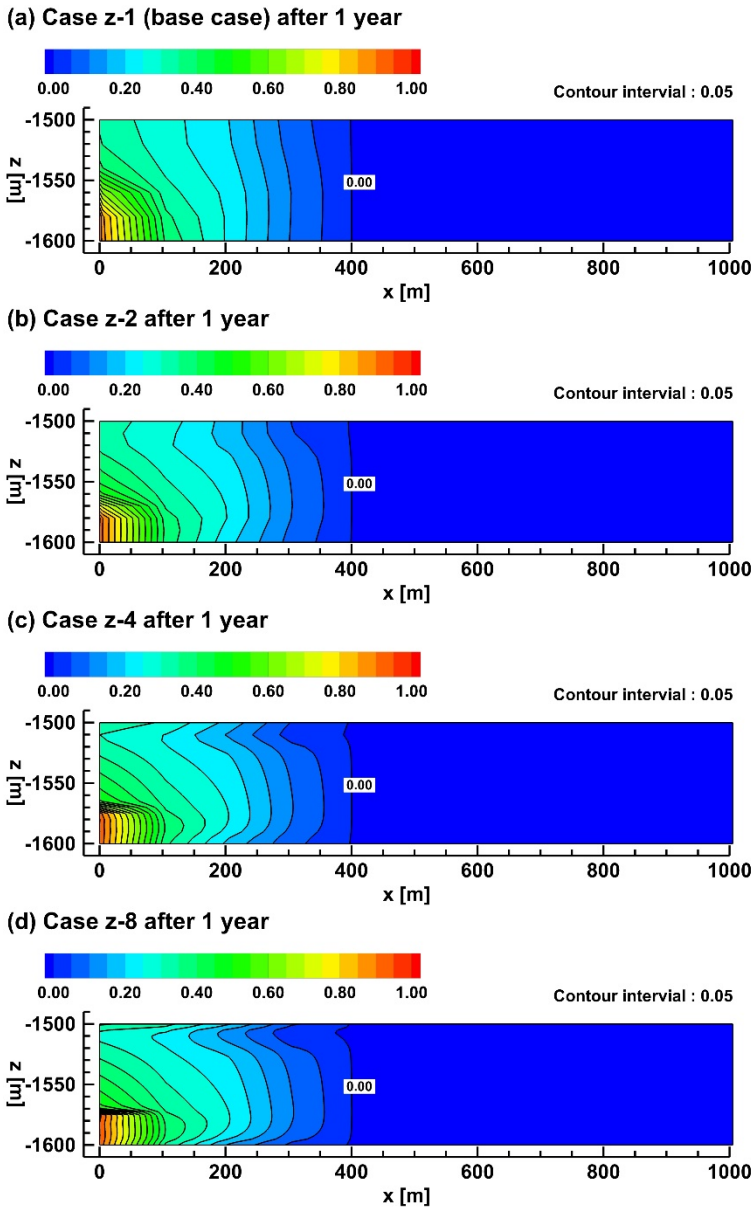

Figure 8. Spatial distributions of saturation of free fluid phase CO_2 in the storage formation after 1 year for (a) base case, (b) Case z-2, (c) Case z-4, (d) Case z-8 since the start of CO_2 injection. Note that this figure is cross section view (y = 0).

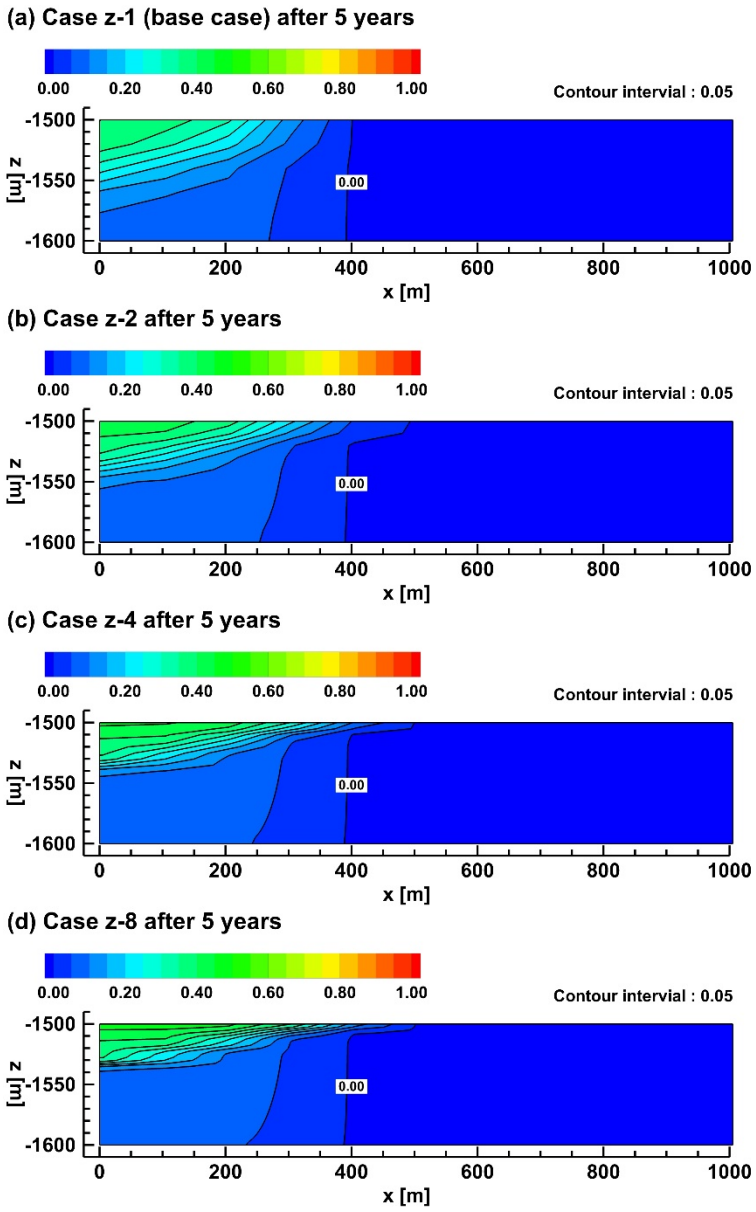

Figure 9. Spatial distributions of saturation of free fluid phase CO_2 in the storage formation after 5 years for (a) base case, (b) Case z-2, (c) Case z-4, (d) Case z-8 since the start of CO_2 injection. Note that this figure is cross section view (y = 0).

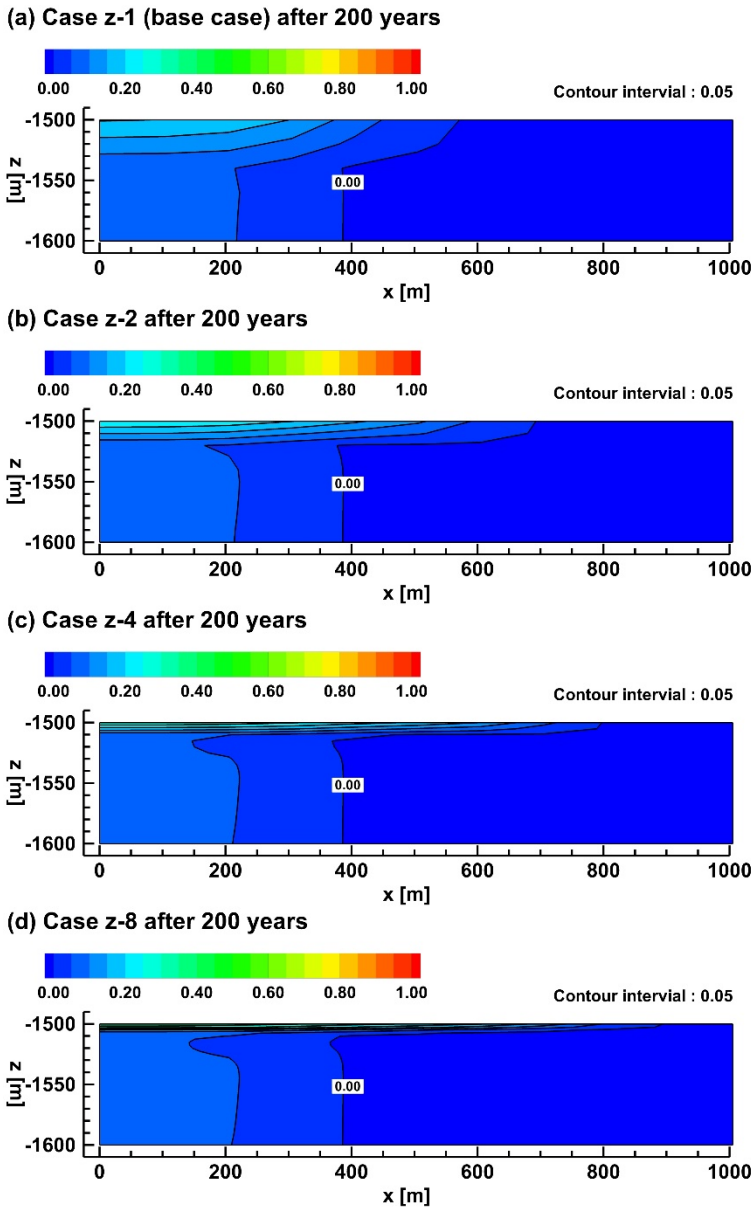

Figure 10. Spatial distributions of saturation of free fluid phase CO_2 in the storage formation after 200 years for (a) base case, (b) Case z-2, (c) Case z-4, (d) Case z-8 since the start of CO_2 injection. Note that this figure is cross section view (y = 0).

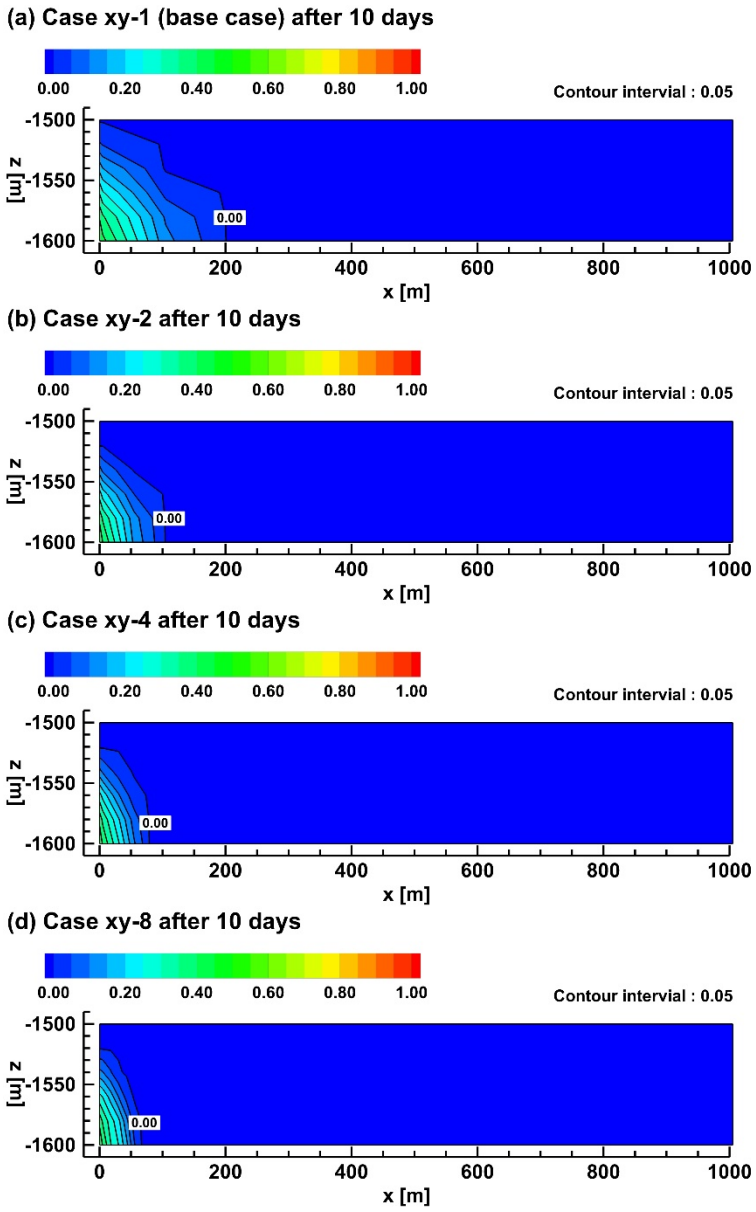

Figure 11. Spatial distributions of saturation of free fluid phase CO_2 in the storage formation after 10 days for (a) base case, (b) Case xy-2, (c) Case xy-4, (d) Case xy-8 since the start of CO_2 injection. Note that this figure is cross section view (y = 0).

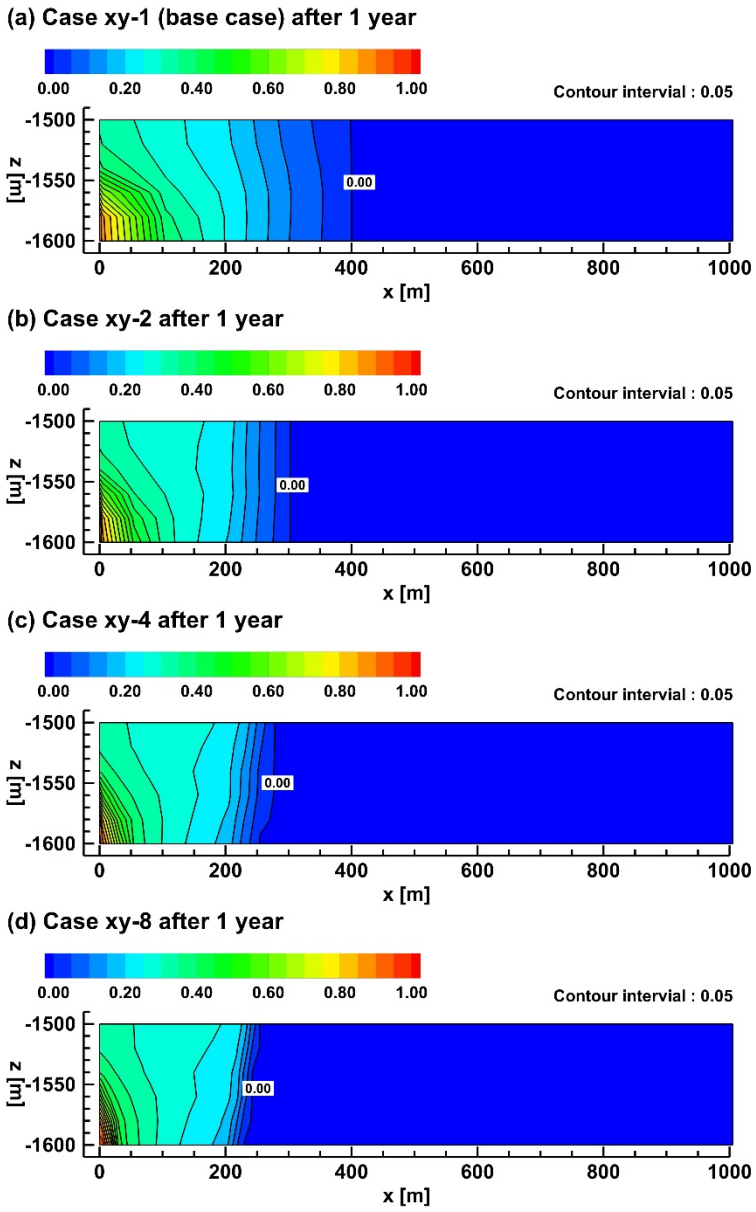

Figure 12. Spatial distributions of saturation of free fluid phase CO_2 in the storage formation after 1 year for (a) base case, (b) Case xy-2, (c) Case xy-4, (d) Case xy-8 since the start of CO_2 injection. Note that this figure is cross section view (y = 0).

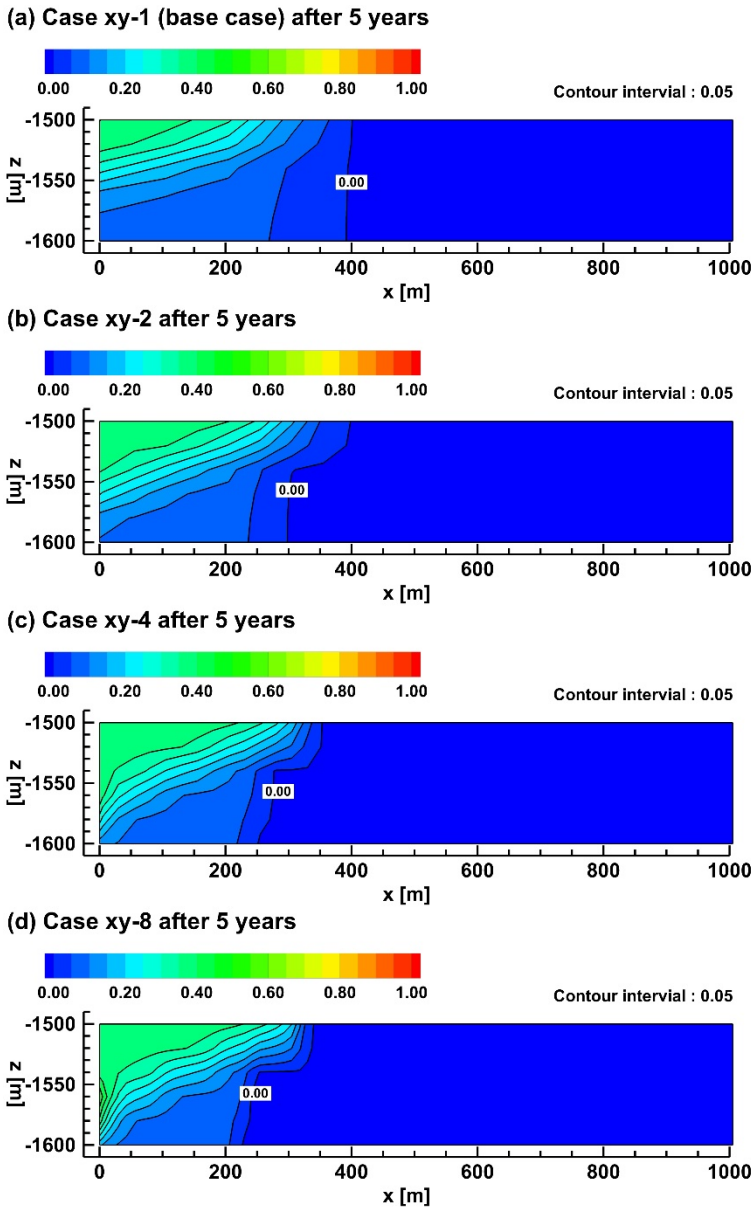

Figure 13. Spatial distributions of saturation of free fluid phase CO_2 in the storage formation after 5 years for (a) base case, (b) Case xy-2, (c) Case xy-4, (d) Case xy-8 since the start of CO_2 injection. Note that this figure is cross section view (y = 0).

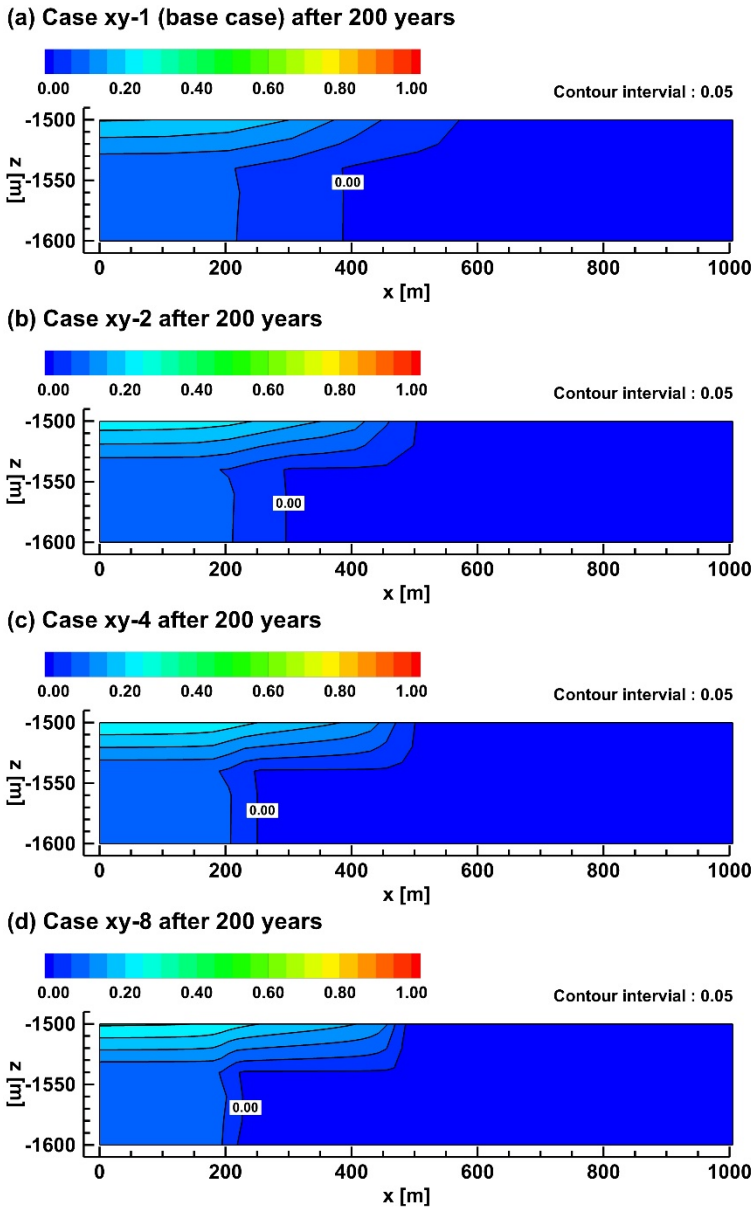

Figure 14. Spatial distributions of saturation of free fluid phase CO_2 in the storage formation after 200 years for (a) base case, (b) Case xy-2, (c) Case xy-4, (d) Case xy-8 since the start of CO_2 injection. Note that this figure is cross section view (y = 0).

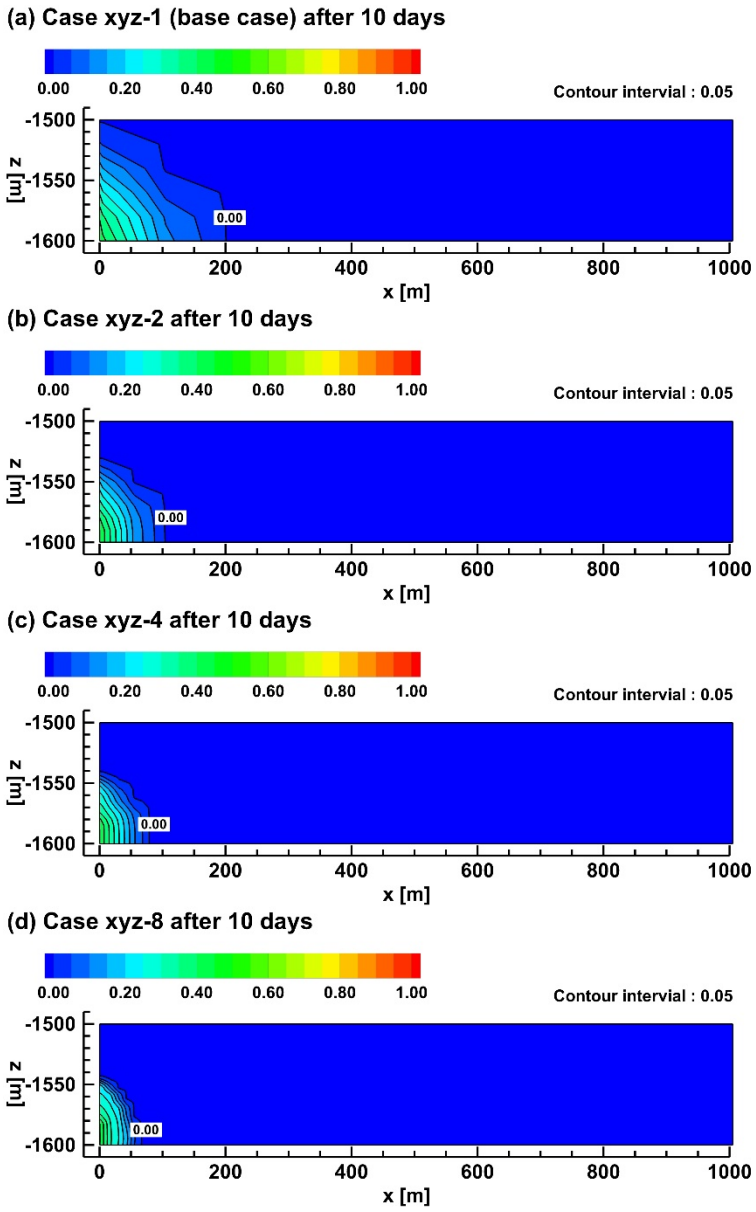

Figure 15. Spatial distributions of saturation of free fluid phase CO_2 in the storage formation after 10 days for (a) base case, (b) Case xyz-2, (c) Case xyz-4, (d) Case xyz-8 since the start of CO_2 injection. Note that this figure is cross section view (y = 0).

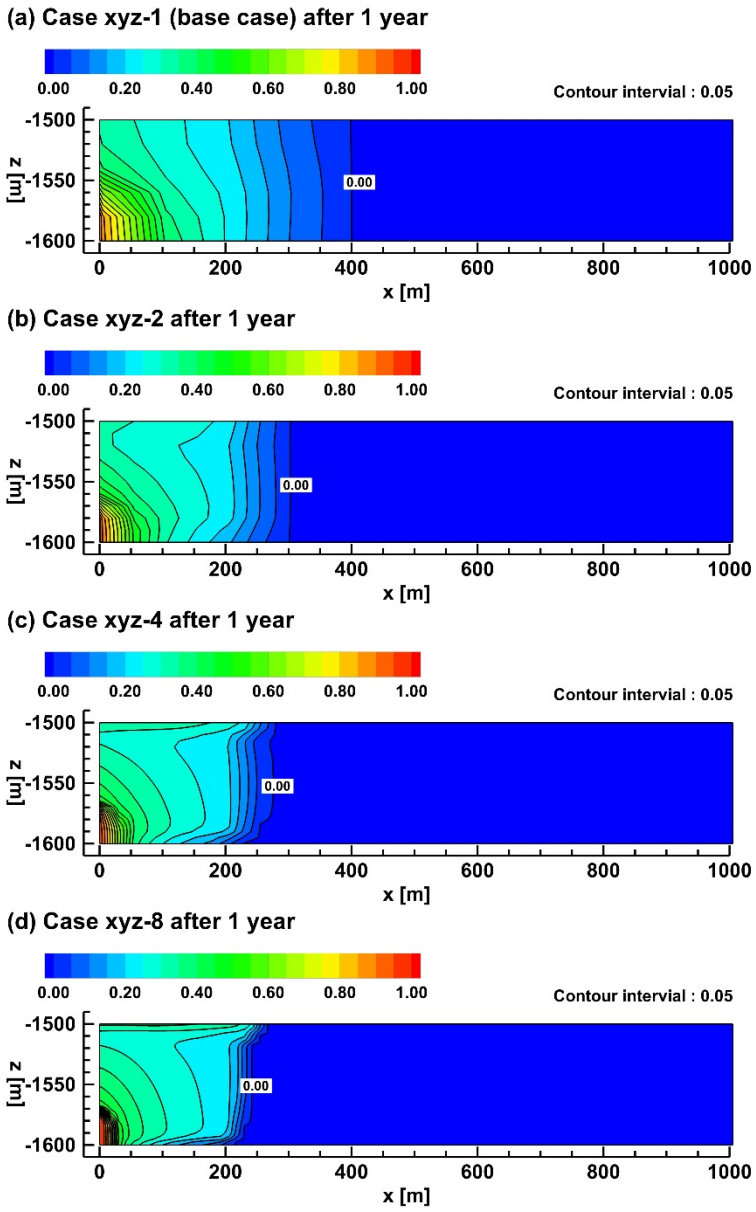

Figure 16. Spatial distributions of saturation of free fluid phase CO_2 in the storage formation after 1 year for (a) base case, (b) Case xyz-2, (c) Case xyz-4, (d) Case xyz-8 since the start of CO_2 injection. Note that this figure is cross section view (y = 0).

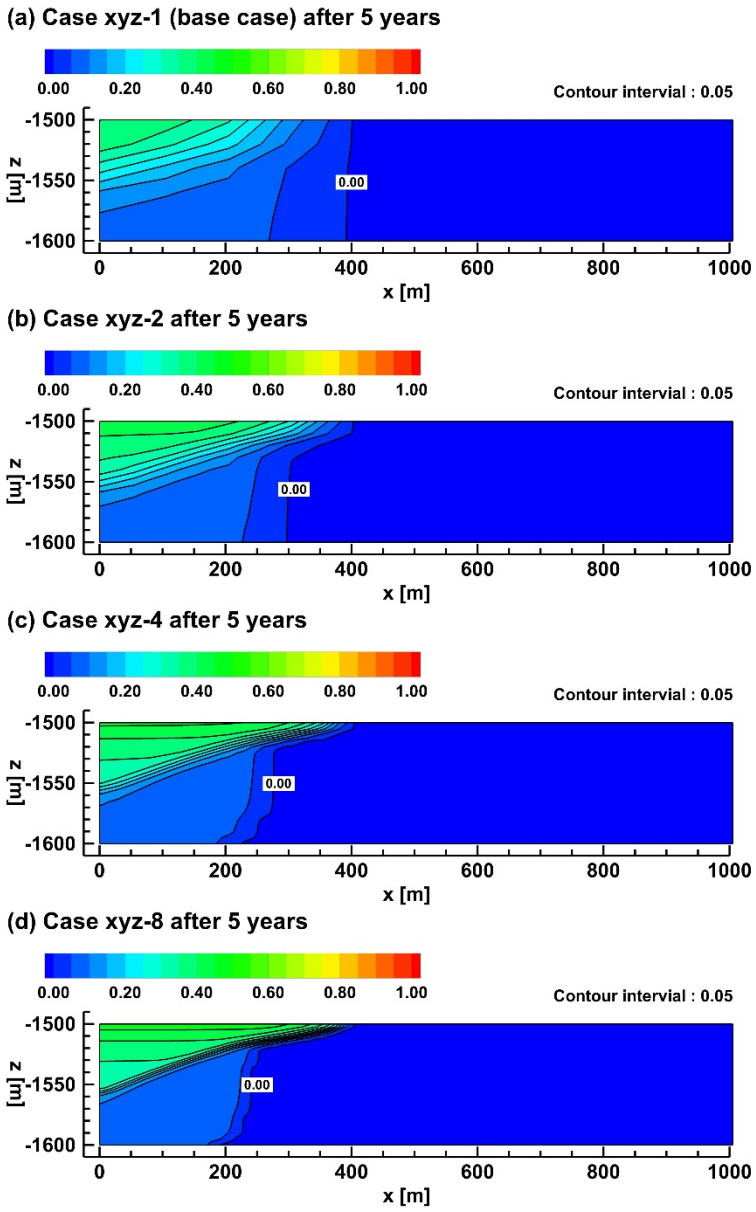

Figure 17. Spatial distributions of saturation of free fluid phase CO_2 in the storage formation after 5 years for (a) base case, (b) Case xyz-2, (c) Case xyz-4, (d) Case xyz-8 since the start of CO_2 injection. Note that this figure is cross section view (y = 0).

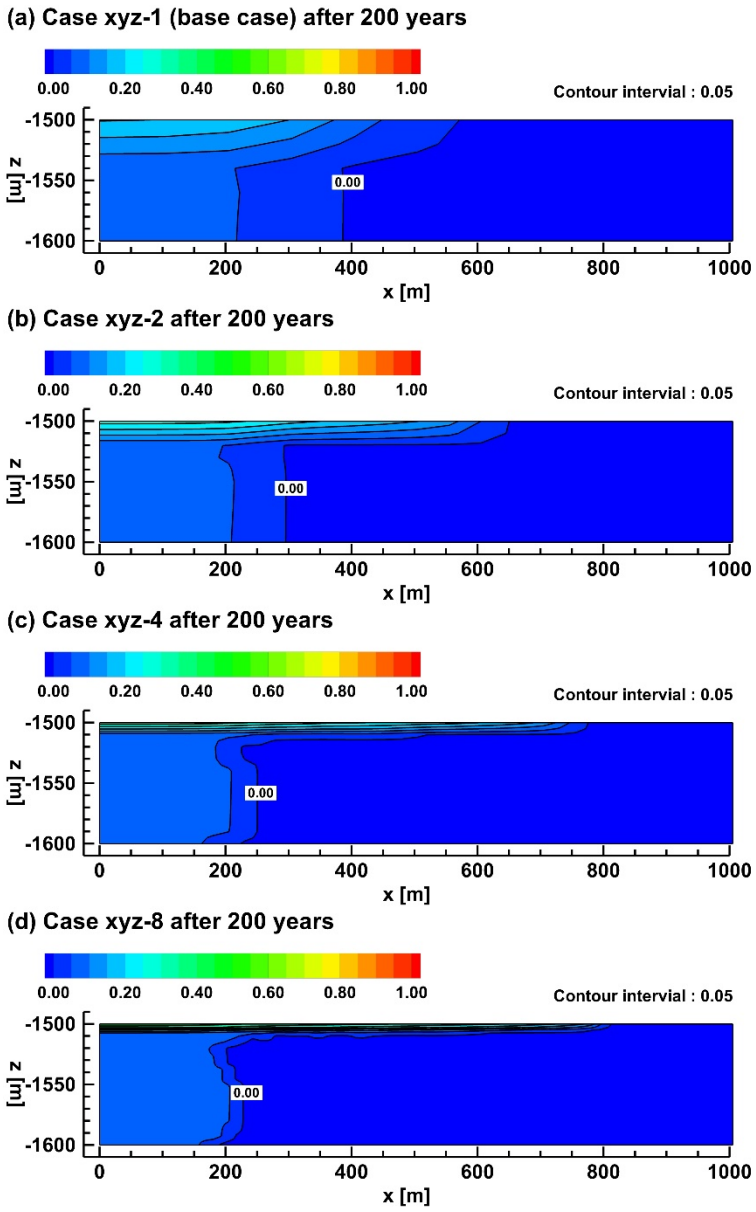

Figure 18. Spatial distributions of saturation of free fluid phase CO_2 in the storage formation after 200 years for (a) base case, (b) Case xyz-2, (c) Case xyz-4, (d) Case xyz-8 since the start of CO_2 injection. Note that this figure is cross section view (y = 0).

4.2. Mass fraction of aqueous phase CO_2

The spatial distributions of mass fraction of aqueous phase CO_2 in the storage formation for Case z including base case after 10 days, 1 year, 5 years, and 200 years in Fig. 19, Fig. 20, Fig. 21, and Fig. 22 respectively. Basically, free fluid phase CO_2 is dissolved into groundwater according to Henry's law. In CO_2 injection period, injected CO_2 rapidly is dissolved into groundwater at the beginning of CO_2 injection and then mass fraction of CO_2 moves due to both migration of free fluid phase CO_2 and displacement of groundwater (Fig. 19 and Fig. 20). However, spatial distributions have difference with grid refinement in vertical direction (Fig. 19a, 19b, 19c, 19d and Fig. 20a, 20b, 20c, 20d). Mass fraction of aqueous phase CO_2 is becomes less underneath cap rock at the beginning of CO_2 injection. Plume (mass fraction group) of aqueous phase CO_2 is changed from bell-shaped to gourd-shaped at the end of CO_2 injection with grid refinement in vertical direction (Fig. 20a, 20b, 20c, 20d). After CO_2 injection is completely finished, mass fraction of aqueous phase CO_2 increases footprint because of migration of free fluid phase CO_2 overall all cases, however, spatial distributions have difference with grid refinement in vertical direction (Fig. 21a, 21b, 21c, 21d and Fig. 22a, 22b, 22c, 22d). Plume of aqueous phase CO_2 underneath obviously becomes thin in vertical direction and laterally presents far along cap rock with grid

refinement in vertical direction (Fig. 21a, 21b, 21c, 21d and Fig. 22a, 22b, 22c, 22d). As a result, radius of aqueous phase CO_2 influence increases at the end of simulation with grid refinement in vertical direction (Fig. 22a, 22b, 22c, 22d).

The spatial distributions of mass fraction of aqueous phase CO_2 in the storage formation for Case xy including base case after 10 days, 1 year, 5 years, and 200 years in Fig. 23, Fig. 24, Fig. 25, and Fig. 26 respectively. In CO_2 injection period, injected CO_2 rapidly dissolved into groundwater at the beginning of CO_2 injection and then mass fraction of CO_2 moves due to both migration of free fluid phase CO_2 and displacement of groundwater (Fig. 23 and Fig. 24). However, spatial distributions have difference with grid refinement in horizontal direction (Fig. 23a, 23b, 23c, 23d and Fig. 24a, 24b, 24c, 24d). Mass fraction of aqueous phase CO_2 is entirely distributed in horizontally narrow space and increases around the screen of injection well with grid refinement in horizontal direction (Fig. 23a, 23b, 23c, 23d and Fig. 24a, 24b, 24c, 24d). As a result, plume of aqueous phase CO_2 is changed from bell-shaped to upside down pyramid-shaped at the end of CO_2 injection with grid refinement in horizontal direction (Fig. 24a, 24b, 24c, 24d). After CO_2 injection is completely finished, mass fraction of aqueous phase CO_2 increases footprint because of migration of free fluid phase CO_2 overall all

cases, however, spatial distributions have difference with grid refinement in horizontal direction (Fig. 25a, 25b, 25c, 25d and Fig. 26a, 26b, 26c, 26d). Mass fraction of aqueous phase CO_2 tends to increase at plume front and then gravity fingering obviously occur at plume front of aqueous phase CO_2 with grid refinement in horizontal direction (Fig. 25a, 25b, 25c, 25d and Fig. 26a, 26b, 26c, 26d).

The spatial distributions of mass fraction of aqueous phase CO_2 in the storage formation for Case xyz including base case after 10 days, 1 year, 5 years, and 200 years in Fig. 27, Fig. 28, Fig. 29, and Fig. 30 respectively. In CO_2 injection period, injected CO_2 rapidly dissolved into groundwater at the beginning of CO_2 injection and then mass fraction of CO_2 moves due to both migration of free fluid phase CO_2 and displacement of groundwater (Fig. 27 and Fig. 28). However, spatial distributions have difference with grid refinement in both directions (Fig. 27a, 27b, 27c, 27d and Fig. 28a, 28b, 28c, 28d). Mass fraction of aqueous phase CO_2 is narrowly distributed in both direction and increases around the screen of injection well at the beginning of CO_2 injection with grid refinement in both directions (Fig. 27a, 27b, 27c, 27d). Mass fraction of aqueous phase CO_2 also presents in horizontally narrow space and increases around the screen of injection as well as plume of aqueous phase CO_2 is changed from bell-shaped to upside down pyramid-shaped at

the end of CO_2 injection with grid refinement in both directions (Fig. 28a, 28b, 28c, 28d). After CO_2 injection is completely finished, mass fraction of aqueous phase CO_2 increases footprint because of migration of free fluid phase CO_2 overall all cases, however, spatial distributions have difference with grid refinement in both directions (Fig. 29a, 29b, 29c, 29d and Fig. 30a, 30b, 30c, 30d). Mass fraction of aqueous phase CO_2 tends to increase at plume front and laterally presents far underneath cap rock with grid refinement in both directions (Fig. 29a, 29b, 29c, 29d and Fig. 30a, 30b, 30c, 30d). In addition, frequency of gravity fingering obviously increases underneath cap rock with grid refinement in both directions, however, gravity fingering does not occur at plume front (Fig. 30a, 30b, 30c, 30d)

The above-mentioned numerical simulation results are interpreted as grid refinement is supposed to accurately consider sharp front and both pressure and temperature in the storage formation. Then, grid refinement affects directly behavior mechanisms of free fluid phase CO_2 as well as indirectly affects behavior mechanisms of groundwater including dissolved CO_2, because dissolved CO_2 into groundwater can change density of groundwater.

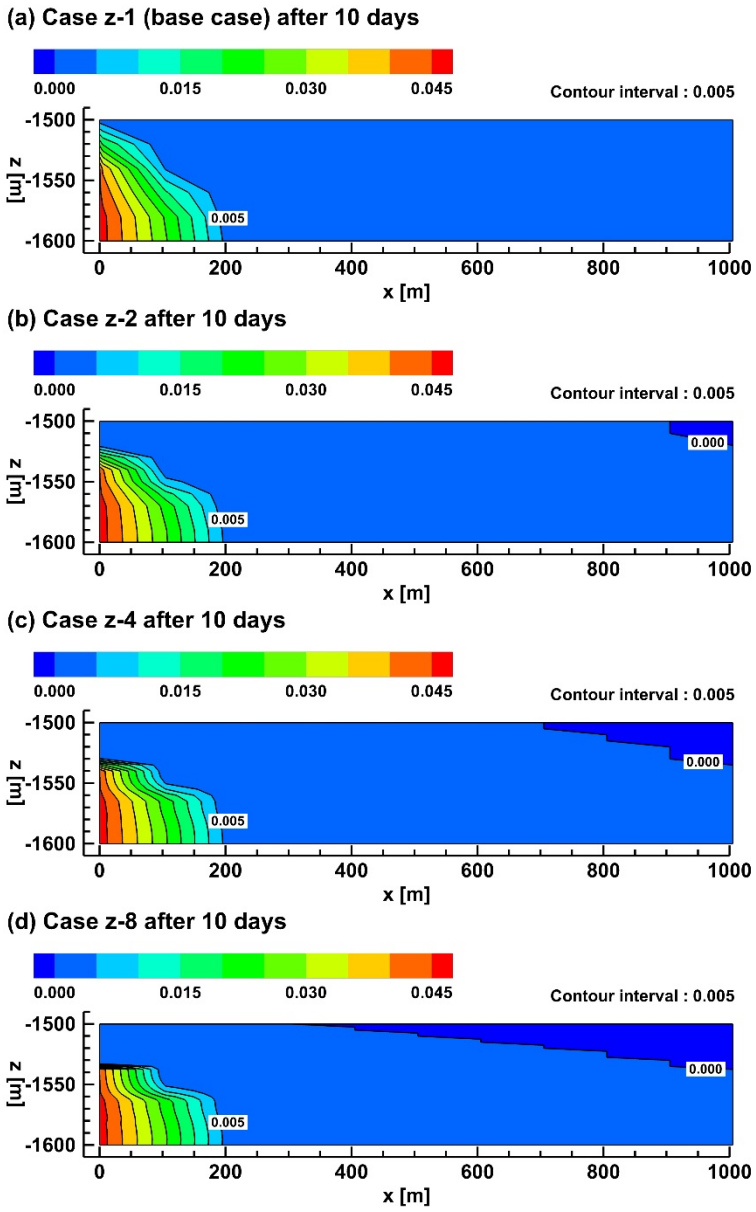

Figure 19. Spatial distributions of mass fraction of aqueous phase CO_2 in the storage formation after 10 days for (a) base case, (b) Case z-2, (c) Case z-4, (d) Case z-8 since the start of CO_2 injection. Note that this figure is cross section view (y = 0).

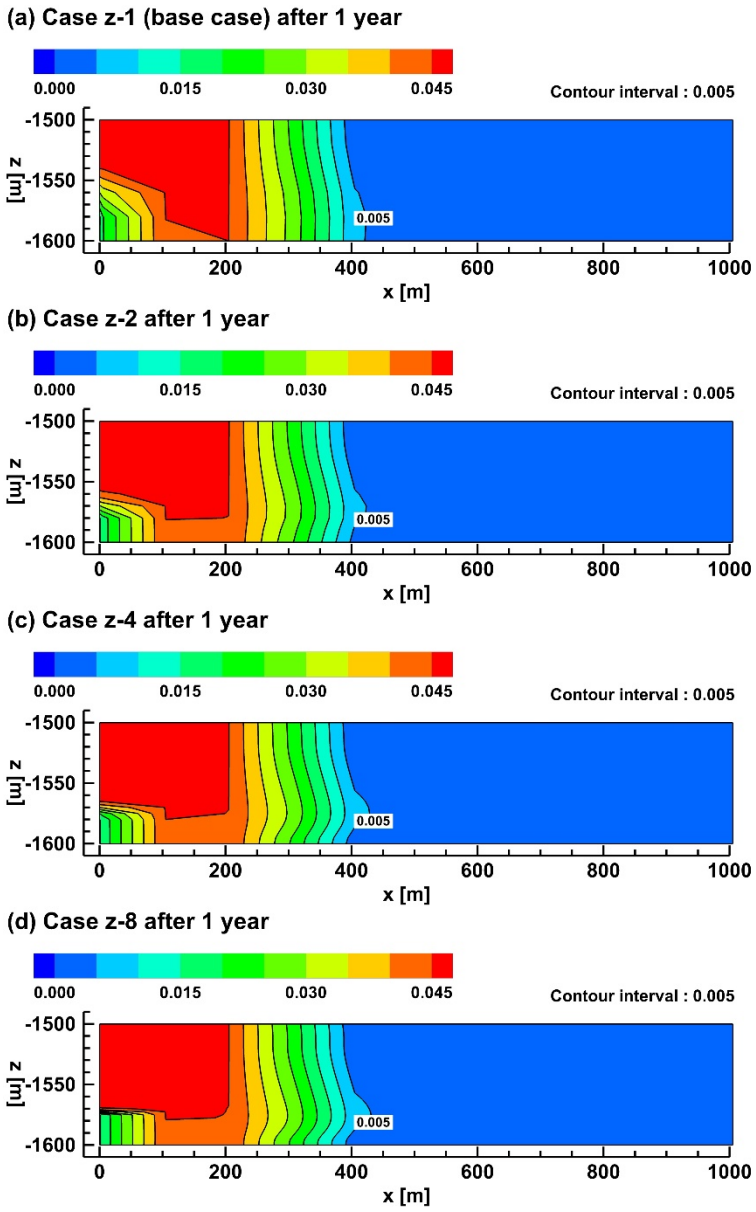

Figure 20. Spatial distributions of mass fraction of aqueous phase CO_2 in the storage formation after 1 year for (a) base case, (b) Case z-2, (c) Case z-4, (d) Case z-8 since the start of CO_2 injection. Note that this figure is cross section view (y = 0).

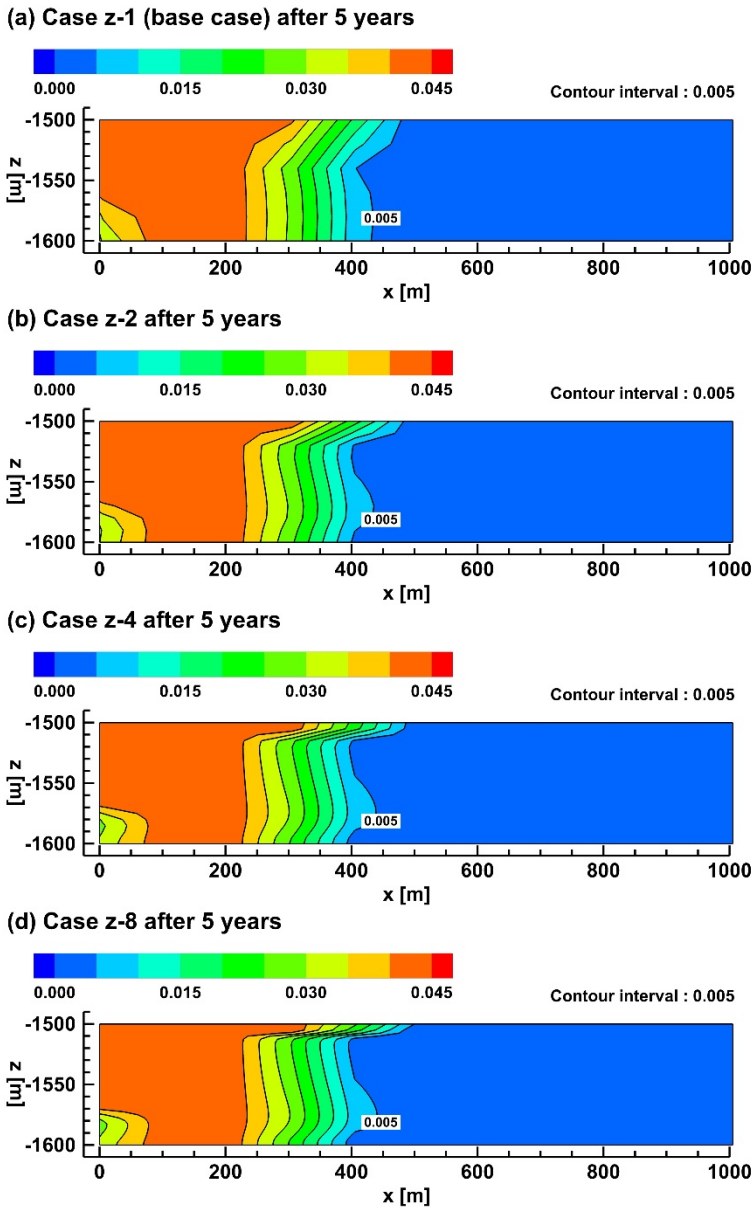

Figure 21. Spatial distributions of mass fraction of aqueous phase CO_2 in the storage formation after 5 years for (a) base case, (b) Case z-2, (c) Case z-4, (d) Case z-8 since the start of CO_2 injection. Note that this figure is cross section view (y = 0).

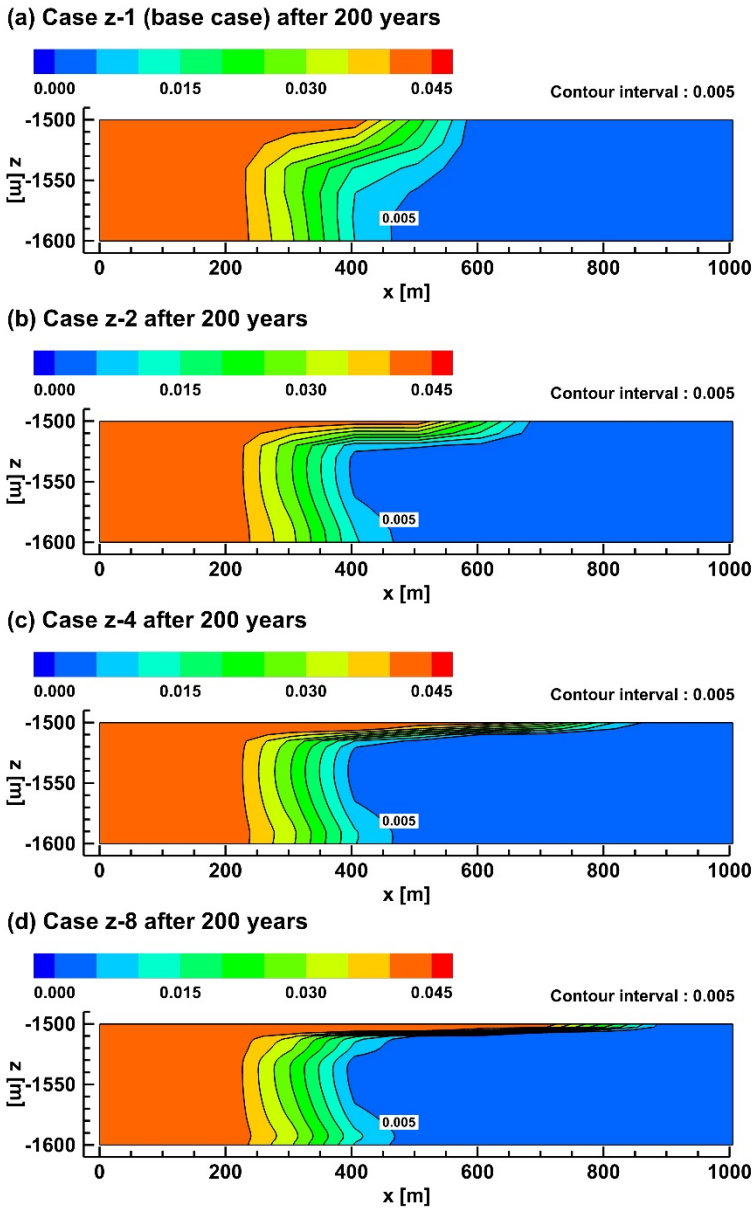

Figure 22. Spatial distributions of mass fraction of aqueous phase CO_2 in the storage formation after 200 years for (a) base case, (b) Case z-2, (c) Case z-4, (d) Case z-8 since the start of CO_2 injection. Note that this figure is cross section view (y = 0).

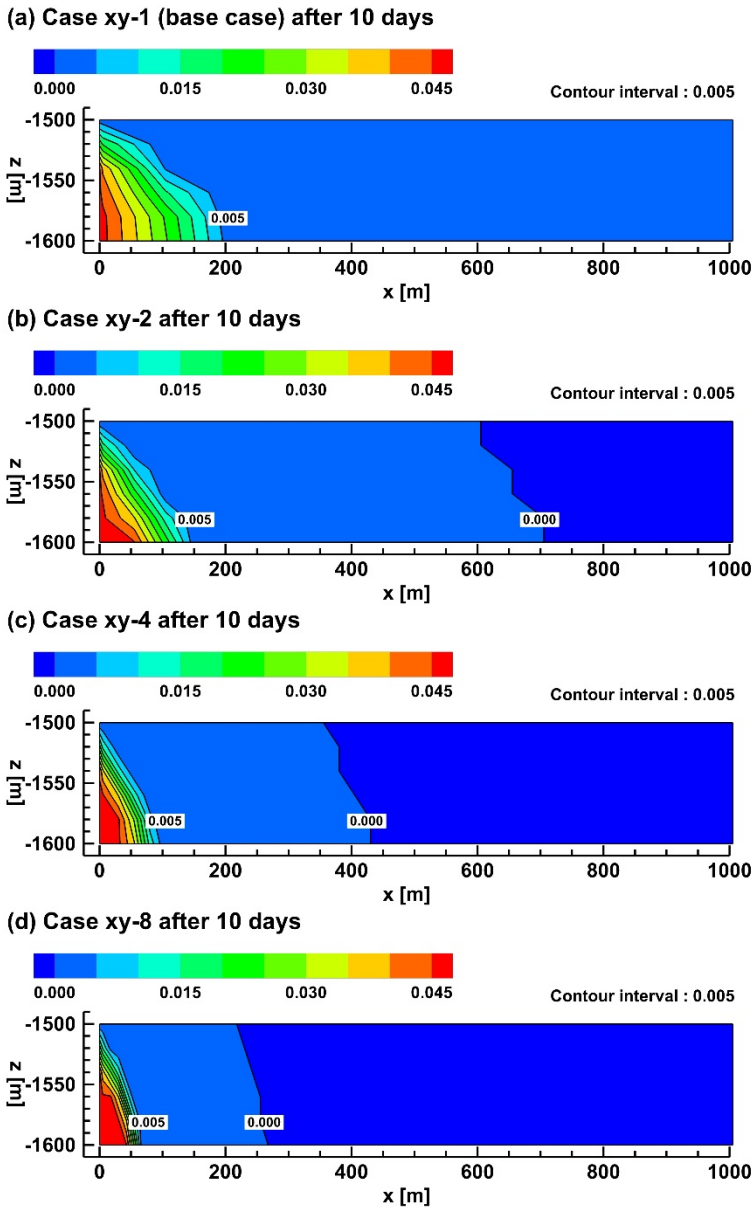

Figure 23. Spatial distributions of mass fraction of aqueous phase CO_2 in the storage formation after 10 days for (a) base case, (b) Case z-2, (c) Case z-4, (d) Case z-8 since the start of CO_2 injection. Note that this figure is cross section view (y = 0).

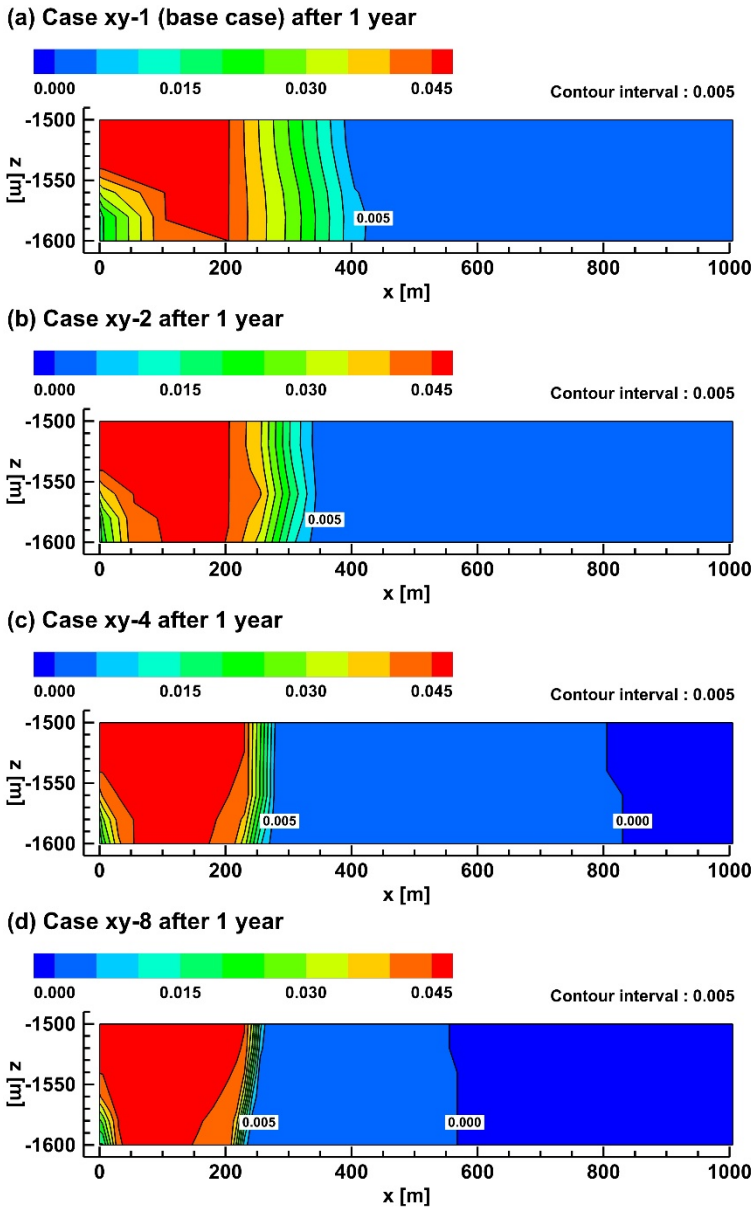

Figure 24. Spatial distributions of mass fraction of aqueous phase CO_2 in the storage formation after 1 year for (a) base case, (b) Case xy-2, (c) Case xy-4, (d) Case xy-8 since the start of CO_2 injection. Note that this figure is cross section view (y = 0).

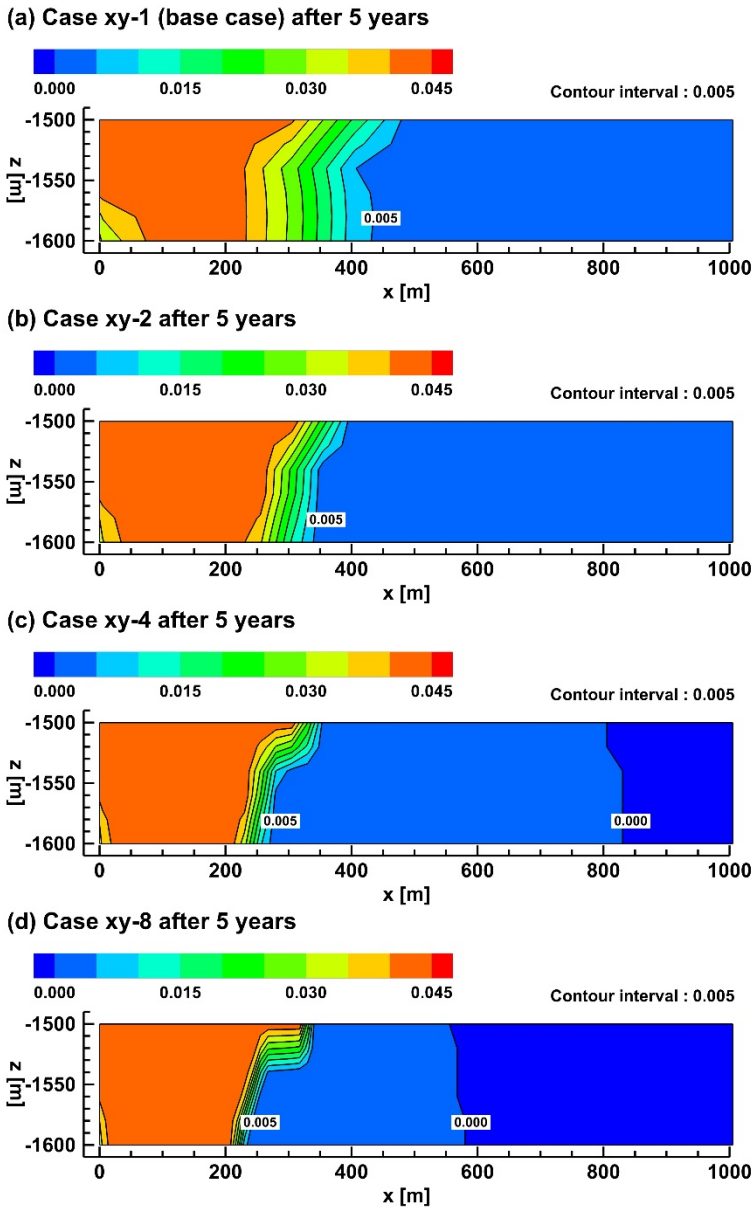

Figure 25. Spatial distributions of mass fraction of aqueous phase CO_2 in the storage formation after 5 years for (a) base case, (b) Case z-2, (c) Case z-4, (d) Case z-8 since the start of CO_2 injection. Note that this figure is cross section view (y = 0).

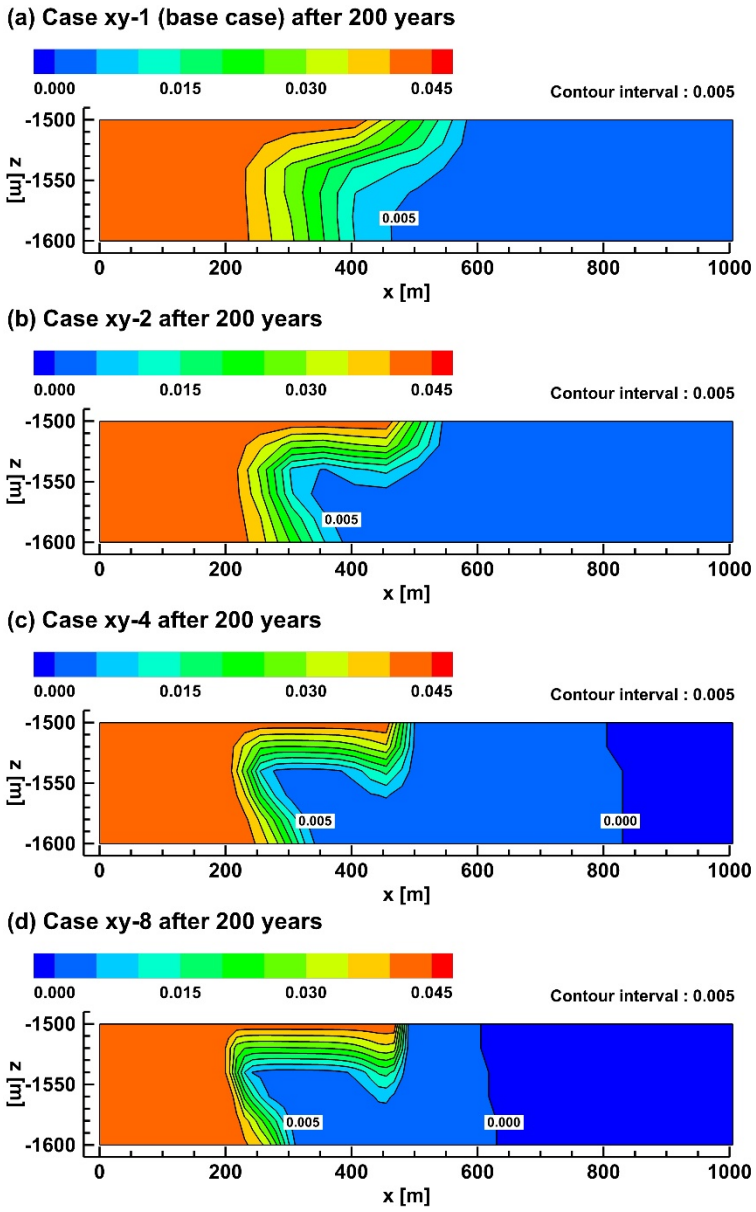

Figure 26. Spatial distributions of mass fraction of aqueous phase CO_2 in the storage formation after 200 years for (a) base case, (b) Case xy-2, (c) Case xy-4, (d) Case xy-8 since the start of CO_2 injection. Note that this figure is cross section view (y = 0).

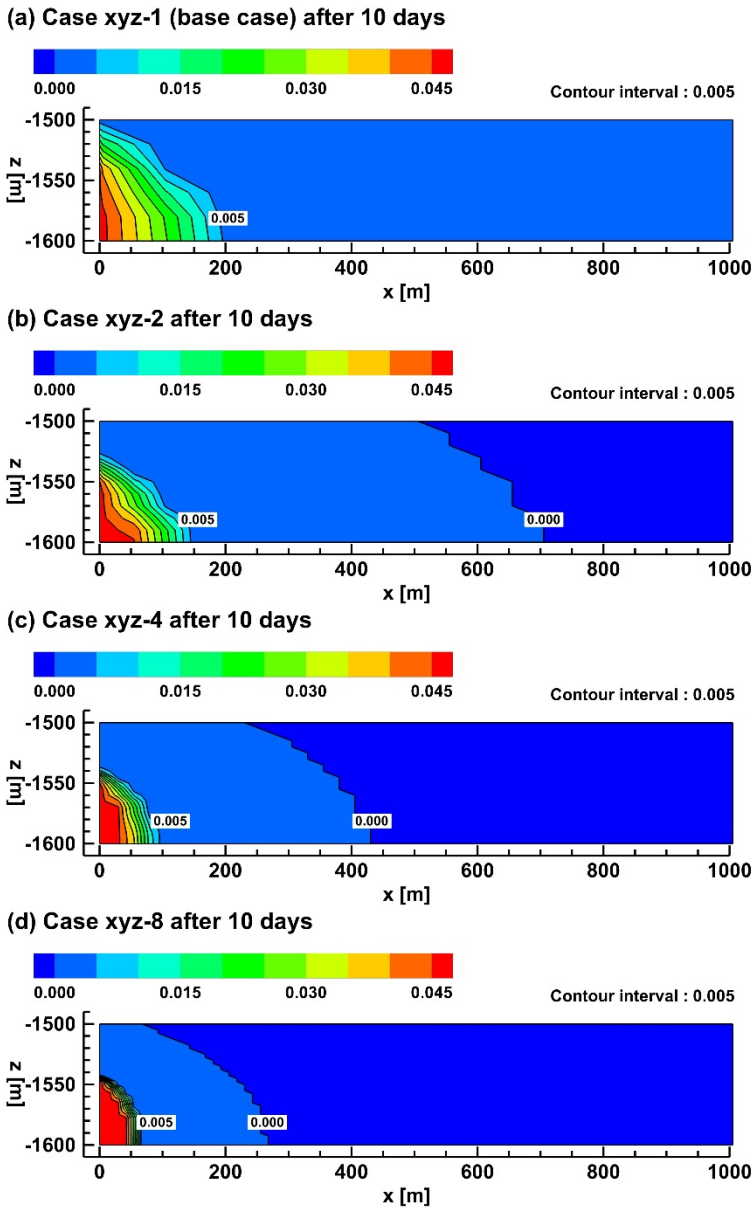

Figure 27. Spatial distributions of mass fraction of aqueous phase CO_2 in the storage formation after 10 days for (a) base case, (b) Case z-2, (c) Case z-4, (d) Case z-8 since the start of CO_2 injection. Note that this figure is cross section view (y = 0).

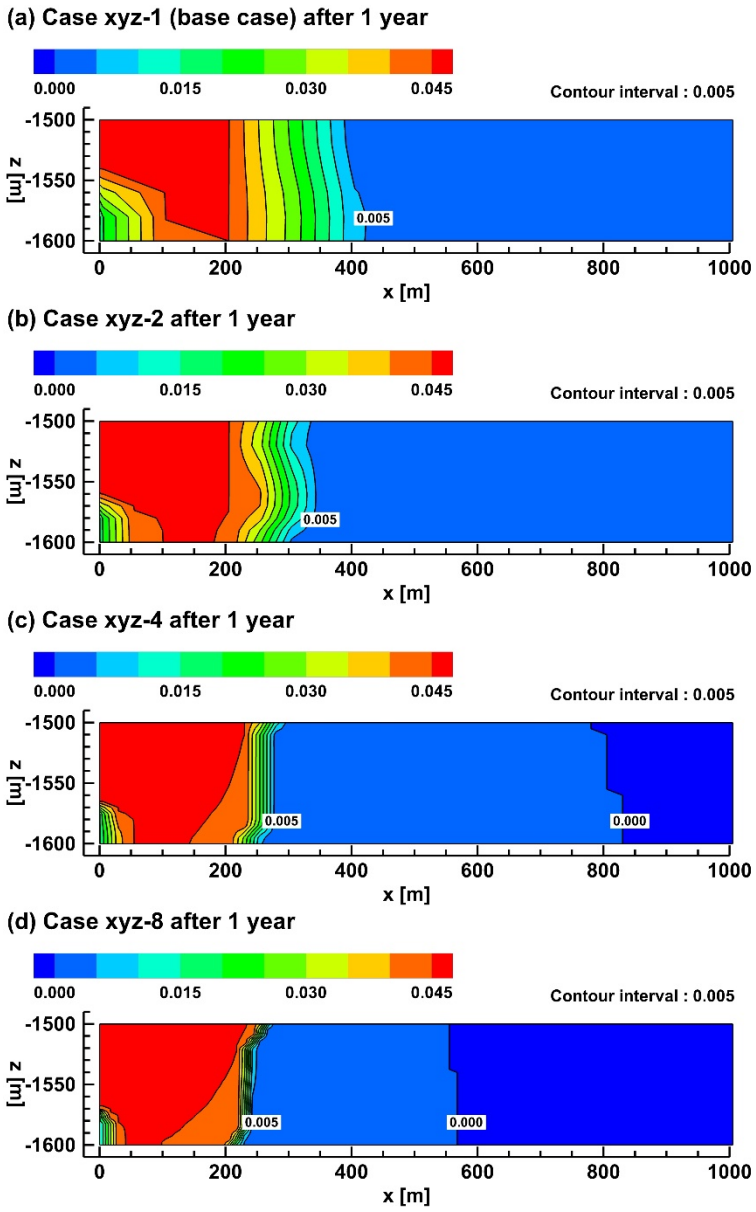

Figure 28. Spatial distributions of mass fraction of aqueous phase CO_2 in the storage formation after 1 year for (a) base case, (b) Case xyz-2, (c) Case xyz-4, (d) Case xyz-8 since the start of CO_2 injection. Note that this figure is cross section view (y = 0).

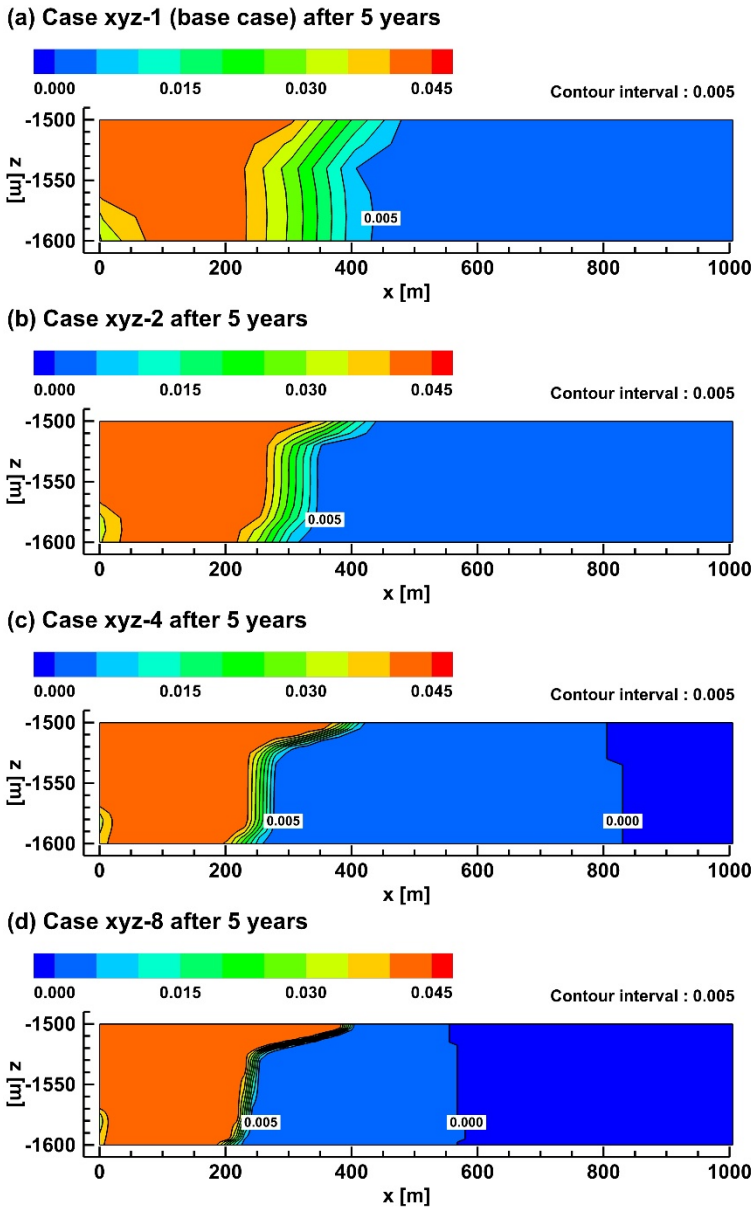

Figure 29. Spatial distributions of mass fraction of aqueous phase CO_2 in the storage formation after 5 years for (a) base case, (b) Case z-2, (c) Case z-4, (d) Case z-8 since the start of CO_2 injection. Note that this figure is cross section view (y = 0).

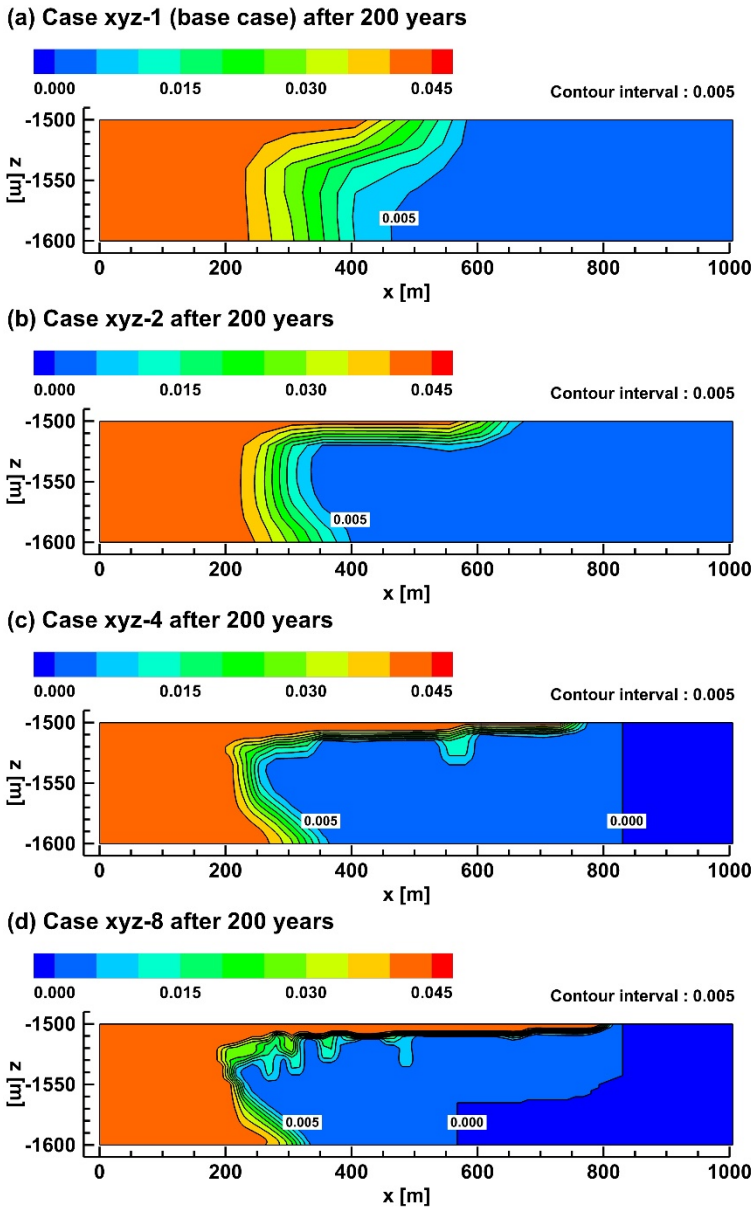

Figure 30. Spatial distributions of mass fraction of aqueous phase CO_2 in the storage formation after 200 years for (a) base case, (b) Case xyz-2, (c) Case xyz-4, (d) Case xyz-8 since the start of CO_2 injection. Note that this figure is cross section view (y = 0).

4.3. Trapping mechanisms efficiency

The temporal changes in the mass fractions of CO_2 stored by hydrodynamic and solubility trapping mechanisms in the storage formation for base case and Case z-8 are illustrated in Fig. 31. Once CO_2 is injected into the storage formation, mass fraction of CO_2 stored by hydrodynamic trapping increases during CO_2 injection period and have 70.84% for base case and 71.04% for Case z-8 at the end of CO_2 injection respectively (Fig 31a, 31b). After CO_2 injection is completed, mass fraction of CO_2 stored by hydrodynamic trapping gradually decreases 52.36% for base case and 50.64% for Case z-8 due to dissolution of CO_2 into groundwater at the end of simulation, whereas mass fraction of CO_2 stored by solubility trapping increases 47.64% for base case and 49.36% for Case z-8 at the end of simulation (Fig 31a, 31b). In other words, grid refinement in vertical direction increases efficiency of hydrodynamic trapping at the end of CO_2 injection, whereas decreases efficiency of hydrodynamic trapping at the end of simulation.

The temporal changes in the mass fractions of CO_2 stored by hydrodynamic and solubility trapping mechanisms in the storage formation for base case and Case xy-8 are illustrated in Fig. 32. Once CO_2 is injected into saline aquifer, mass fraction of CO_2 stored by hydrodynamic trapping

increases during CO_2 injection period and have 70.84% for base case and 82.04% for Case xy-8 at the end of CO_2 injection respectively (Fig 32a, 32b). After CO_2 injection is completed, mass fraction of CO_2 stored by hydrodynamic trapping gradually decreases 52.36% for base case and 61.22% for Case xy-8 due to dissolution of CO_2 into groundwater at the end of simulation, whereas mass fraction of CO_2 stored by solubility trapping increases 47.64% for base case and 38.78% for Case xy-8 at the end of simulation (Fig 32a, 32b). In other words, grid refinement in horizontal direction increases efficiency of hydrodynamic trapping at the end of CO_2 injection as well as increases efficiency of hydrodynamic trapping at the end of simulation.

The temporal changes in the mass fractions of CO_2 stored by hydrodynamic and solubility trapping mechanisms in the storage formation for base case and Case xyz-8 are illustrated in Fig. 33. Once CO_2 is injected into saline aquifer, mass fraction of CO_2 stored by hydrodynamic trapping increases during CO_2 injection period and have 70.84% for base case and 82.21% for Case xyz-8 at the end of CO_2 injection respectively (Fig 33a, 33b). After CO_2 injection is completed, mass fraction of CO_2 stored by hydrodynamic trapping gradually decreases 52.36% for base case and 56.35% for Case xyz-8 due to dissolution of CO_2 into groundwater at the end of

simulation, whereas mass fraction of CO_2 stored by solubility trapping increases 47.64% for base case and 43.65% for Case xyz-8 at the end of simulation (Fig 33a, 33b). In other words, grid refinement in both directions increases efficiency of hydrodynamic trapping at the end of CO_2 injection as well as increases efficiency of hydrodynamic trapping at the end of simulation.

The changes in trapping efficiency difference of CO_2 between 1 year and 200 years are illustrated in Fig. 34. Trapping efficiency difference of CO_2 increases 18.48% to 20.39% with grid refinement in vertical direction (Fig 34a). Trapping efficiency difference of CO_2 increases 18.48% to 20.82% with grid refinement in horizontal direction, however, Case xy-4 is bigger than Case xy-8 (Fig 34b). Trapping efficiency difference of CO_2 increases 18.48% to 25.86% with grid refinement in both directions (Fig 34c).

The above-mentioned numerical simulation results suggest that efficiency of trapping mechanisms are dependent on behavior of both CO_2 and groundwater. According to behavior of multi-phase fluid, grid refinement enhances efficiencies of hydrodynamic trapping and reduces solubility trapping due to accurate consideration of sharp front in whole simulation time. However, grid refinement in vertical direction reduces efficiencies of hydrodynamic trapping and enhances solubility trapping due to increase of space, where CO_2 and groundwater co-exists in whole simulation time.

Meanwhile, grid refinement increases efficiency difference of hydrodynamic trapping during injection period because of increase of saturation due to accurate consideration of sharp front. However, grid refinement enhances efficiency difference of solubility trapping after injection is completed because of boost of multi-phase fluid flow due to increase of saturation and accurate consideration of both pressure and temperature in the storage formation. However, efficiency difference of solubility trapping after injection is completed decreases due to CO_2 tailing near injection well in Case xy-8. It may be summarized with that grid refinement in horizontal direction enhances efficiency of hydrodynamic trapping in CO_2 injection period, whereas grid refinement in vertical direction enhances efficiency of solubility trapping after CO_2 injection is finished.

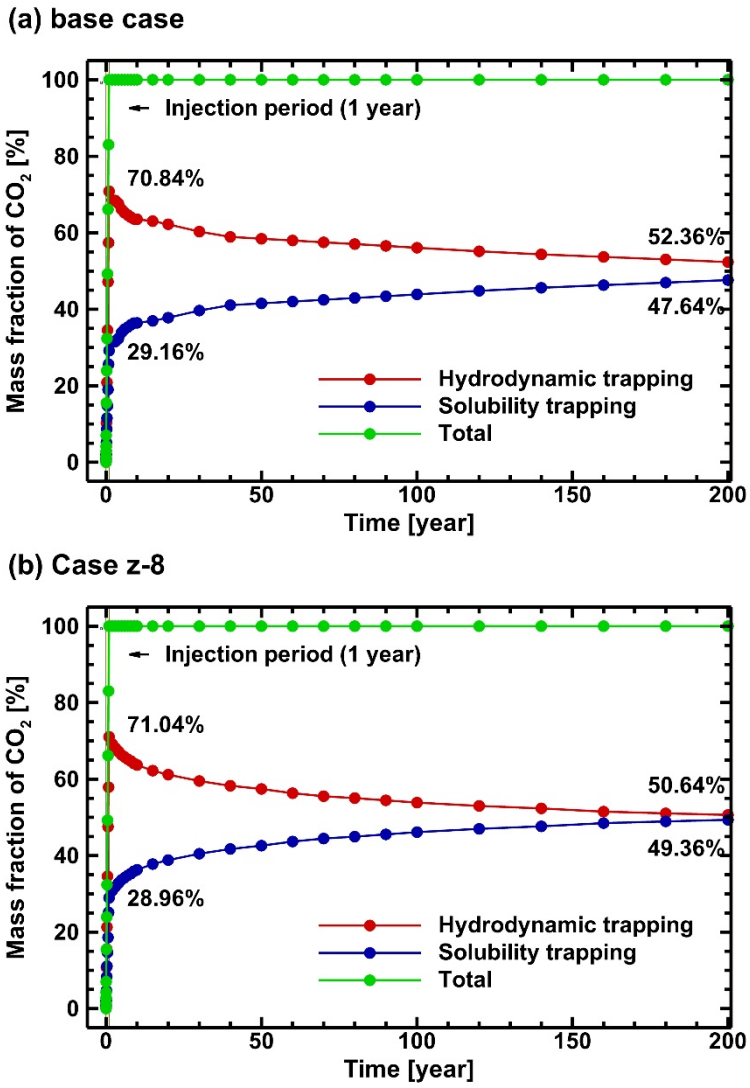

Figure 31. Temporal changes in mass fractions of CO_2 stored by hydrodynamic and solubility trapping mechanisms in the storage formation for (a) base case and (b) Case z-8.

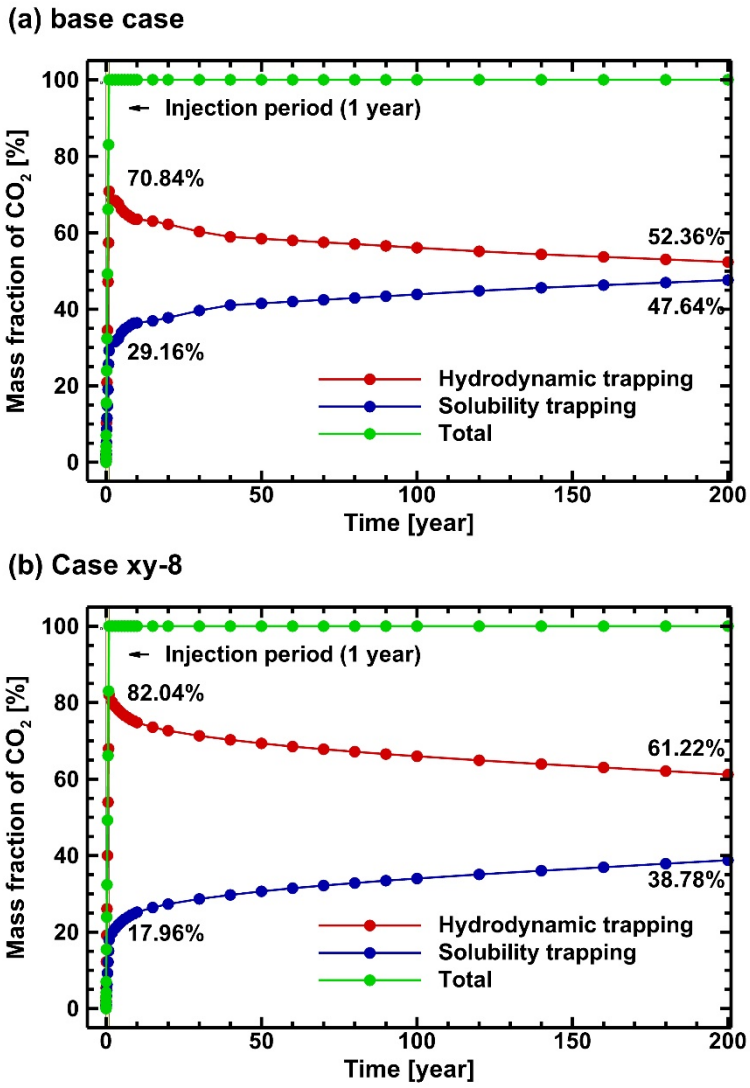

Figure 32. Temporal changes in mass fractions of CO_2 stored by hydrodynamic and solubility trapping mechanisms in the storage formation for (a) base case and (b) Case xy-8.

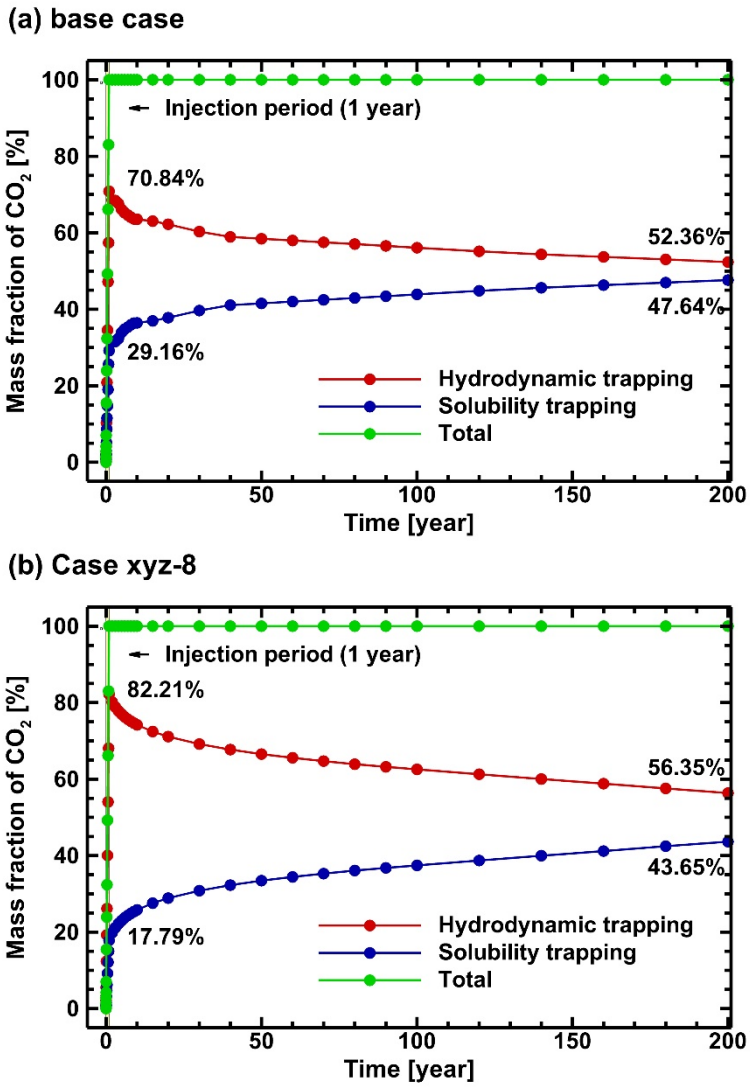

Figure 33. Temporal changes in mass fractions of CO_2 stored by hydrodynamic and solubility trapping mechanisms in the storage formation for (a) base case and (b) Case xyz-8.

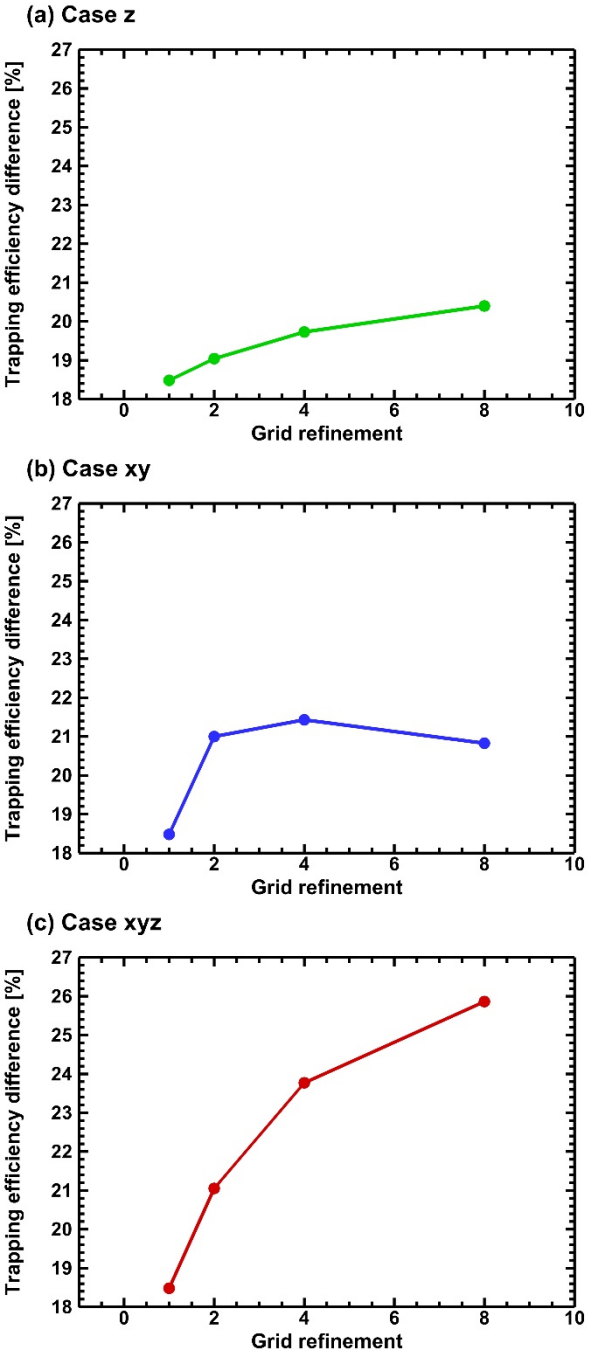

Figure 34. Changes in trapping efficiency difference of CO_2 between 1 year and 200 years with grid refinement.

5. Discussions

As mentioned above, grid refinement is supposed to accurately consider pressure and temperature in the storage formation. As a result, grid refinement affects directly behavior mechanisms of free fluid phase CO_2 as well as indirectly affect both behavior mechanisms of groundwater including dissolved CO_2 and trapping mechanisms. Although temperature around injection well can change due to injected CO_2 into storage formations (Kihm, 2012), isothermal is considered in this study. Thus a further study is suggested as follows. Impacts of grid refinement on behavior and trapping mechanisms of injected CO_2 should be comprehensively evaluated in non-isothermal condition.

6. Conclusions

A series of numerical simulation using a multi-phase thermo-hydro numerical model is performed to analyze and evaluate impacts of grid refinement in each individual direction and both directions on behavior and trapping mechanisms of injected CO_2 into a hypothetical deep storage formation. First of all, the modeling domain is then discretized into base case. Then it is further discretized into a half, a quarter, and one-eighth in each individual direction and both directions. The results of numerical simulation show that behavior (both free fluid phase and aqueous phase CO_2) and trapping mechanisms (hydrodynamic and solubility) of injected CO_2 are significant to grid refinement in each individual direction and both directions. This is largely related with multi-phase system where CO_2 (gas) is suddenly injected into liquid almost saturated storage formations. Another reason is related with large compressibility of CO_2 even in deep storage formations. It is found that grid refinement regardless of direction basically reduces behavior of injected CO_2 due to accurate consideration of sharp front. Since CO_2 horizontally moves due to pressure gradient in CO_2 injection period and CO_2 vertically moves due to buoyancy after injection is finished, grid refinement in horizontal direction largely affects behavior of injected CO_2 in CO_2 injection period, whereas grid refinement in vertical direction mainly

affects behavior of injected CO_2 after CO_2 injection is finished. As a result, injected CO_2 with grid refinement in both directions apparently moves like behavior of injected CO_2 with grid refinement in horizontal direction in CO_2 injection period, whereas it apparently moves like behavior of injected CO_2 in vertical direction after CO_2 injection is finished. Likewise, hydrodynamic trapping is mainly enhanced by grid refinement in horizontal direction in CO_2 injection period, whereas solubility trapping is mainly enhanced by grid refinement in vertical direction after CO_2 injection is finished. However, efficiency difference of trapping mechanisms (between 1 year and 200 years) shows that grid refinement in both directions is not simple superposition of impacts of both each individual direction, but seems like synergy of their impacts. Therefore, it may be concluded that a modeling domain must be discretized into proper grid size in both directions when more rigorous and reasonable predictions of thermo-hydro responses of the geologic of CO_2 storage and its trapping mechanisms are to be obtained using a multi-phase thermo-hydro numerical model. In this sense, this study can provide reasonable guideline for planning of geologic storage of carbon dioxide as a fundamental research. Further numerical studies considering non-isothermal are recommend to arrive at more general conclusions.

References

Computer Modelling Group, 2009, GEM user's guide, version 2009: Advanced compositional and GHG reservoir simulator. Technical Report, Computer Modelling Group (CMG), Calgary, Alberta, Canada, 1123 p.

Corey, A.T., 1954, The interrelation between gas and oil relative permeabilities. Producers Monthly, 19 (November), 38-41.

Doughty, C. and Pruess, K., 2004, Modeling supercritical carbon dioxide injection in heterogeneous porous media. Vadose Zone Journal, 3, 837-847.

Holloway, S., 1997, An overview of the underground disposal of carbon dioxide. Energy Conversion and Management, 38, 193-198.

Hosa, A., Esentia, M., Stewart, J. and Haszeldine, S., 2011, Injection of CO_2 into saline formations: Benchmarking worldwide projects. Chemical Engineering Research and Design, 89, 1855-1864.

Johnson J.W., Nitao, J.J. and Knauss, K.G., 2004, Reactive transport modeling of CO_2 storage in saline aquifers to elucidate fundamental processes, trapping mechanisms, and sequestration partitioning. In: Baines, S.J. and Worden, R.H. (eds.), Geological Storage of Carbon Dioxide, Special Publications, No. 233. Geological Society of London, UK, 107-128.

Karypsis, G., 2013, METIS, version 5.1.0: A software package for partitioning unstructured graphs, partitioning meshes, and computing fill-reducing orderings of sparse matrices. Technical Report, Department of Computer Science and Engineering, University of Minnesota, Minneapolis, Minnesota, USA, 35 p.

Kihm, J.H., 2012, Application of integrated numerical modeling technologies for geologic storage of carbon dioxide. Ph.D. thesis, Seoul National University, Seoul, Korea, 157 p.

Kihm, J.H. and Kim, J.M., 2007, Numerical simulation of behavior characteristics and trapping mechanisms of carbon dioxide injected into a deep saline aquifer for geologic storage. Annual Conference of the Geological Society of Korea (Abstracts), Chuncheon, October 25-26, (in Korean).

Kihm, J.H. and Kim, J.M., 2008, Numerical simulation of thermo-hydro-mechanical stability evaluation of carbon dioxide geologic storage with various characteristics of geologic structures and injection locations. Annual Conference of the Korean Society of Economic and Environmental Geology (Abstracts), Seoul, April 23-25, (in Korean).

Kihm, J.H., Kim, J.M., Wang, S. and Xu, T., 2012a, Hydrogeochemical numerical simulation of impacts of mineralogical compositions and convective fluid flow on trapping mechanisms and efficiency of carbon

dioxide injected into deep saline sandstone aquifers. Journal of Geophysical Research, 117, B06204.

Kihm, J.H., Park, S.U. and Kim, J.M., 2012b, Evaluation of carbon dioxide plume injected in the Gyeongsang Basin, Korea. Second Korea CCS Conference (Abstracts), Jeju, March 14-16 (in Korean).

Kim, J.M., 2008, Development and application of a fully coupled multiphase numerical model for thermo-hydro-mechanical analysis of optimal geologic sequestration of carbon dioxide. Final Report M102KP010017-07K1601-01710, Seoul National University, Seoul, Korea, 131 p (in Korean with English summary).

Kim, J.M., 2009, Development and field validation of characterization, drilling, injection, and prediction technologies for geologic sequestration of carbon dioxide. Annual Report 16-2008-08-001-00, Seoul National University, Seoul, Korea, 128 p (in Korean with English summary).

Kim, J.M., 2014, Development of integrated numerical modeling technologies for predicting behavior of geologically injected carbon dioxide. Final Report 2013M1A8A1035824, Seoul National University, Seoul, Korea, 202 p (in Korean with English summary).

Lindeberg, E., Vuillaume, J.F. and Ghaderi, A., 2009, Determination of the CO_2 storage capacity of the Utsira formation. Energy Procedia, 1, 2777-2784.

Litynski, J., Rodosta, T. and Brown, B., 2012, Best practices for monitoring, verification, and accounting of CO_2 stored in deep geologic formations - 2012 update, second edition. Technical Report DOE/NETL-2012/1568, National Energy Technology Laboratory, Washington, DC, USA, 136 p.

Mansell, R.S., Ma, L., Ahuja, L.R., and Bloom, S.A., 2002, Adaptive grid refinement in numerical models for water flow and chemical transport in soil: A review. Vadose Zone Journal, 1, 222-238.

Metz, B., Davison, O., de Coninck, H.C., Loos, M. and Mayer, L.A. (eds.), 2005, Intergovernmental Panel on Climate Change Special Report on Carbon Dioxide Capture and Storage. Cambridge University Press, Cambridge, UK, 431 p.

Narasimhan, T.N. and Witherspoon, P.A., 1976, An integrated finite difference method for analyzing fluid flow in porous media. Water Resources Research, 12, 57-64.

Park, S.U., Kihm, J.H. and Kim, J.M., 2011, Evaluation of land deformation and stability changes due to geologic storage of carbon dioxide using a thermo-hydro-mechanical numerical model. First Korea CCS Conference (Abstracts), Jeju, April 13-15 (in Korean).

Pruess, K., Oldenburg, C. and Moridis, G., 1999, TOUGH2 user's guide, version 2.0. Technical Report LBNL-43134, Lawrence Berkeley

National Laboratory, University of California, Berkeley, California, USA, 198 p.

Rutqvist, J., Wu, Y.S., Tsang, C.F. and Bodvarsson, G., 2002, A modeling approach for analysis of coupled multiphase fluid flow, heat transfer, and deformation in fractured porous rock. International Journal of Rock Mechanics and Mining Sciences, 39, 429-442.

Scottish Carbon Capture and Storage, 2011, Progressing Scotland's CO_2 storage opportunities. Technical Report, Scottish Carbon Capture and Storage (SCCS), Edinburgh, UK, 60 p.

Smith, D.J., Noy, D.J., Holloway, S. and Chadwick, R.A., 2011, The impact of boundary conditions on CO_2 storage capacity estimation in aquifers. Energy Procedia, 4, 4828-4834.

Spycher, N. and Pruess, K., 2005, CO_2-H_2O mixtures in the geological sequestration of CO_2, II. Partitioning in chloride brines at 12-100°C and up to 600 bar. Geochimica et Cosmochimica Acta, 69, 3309-3320.

van Genuchten, M.Th., 1980, A closed-form equation for predicting the hydraulic conductivity of unsaturated soils. Soil Science Society of America Journal, 44, 892-898.

White, S.P., Allis, R.G., Moore, J., Chidsey, T., Morgan, C., Gwynn, W. and Adams, M., 2005, Simulation of reactive transport of injected CO_2 on the Colorado Plateau, Utah, USA. Chemical Geology, 217, 387-405.

White, M.D. and Oostrom, M., 2006, STOMP user's guide: Subsurface transport over multiple phases, version 4.0. Technical Report PNNL-15782, Pacific Northwest National Laboratory, Richland, Washington, USA, 108 p.

Xu, T., Spycher, N., Sonnenthal, E., Zheng L. and Pruess, K., 2012, TOUGHREACT user's guide: A simulation program for non-isothermal multiphase reactive transport in variably saturated geologic media, version 2.0. Technical Report LBNL-DRAFT, Lawrence Berkeley National Laboratory, University of California, Berkeley, California, USA, 240 p.

Xu, T., Zheng, L. and Tian, H., 2011, Reactive transport modeling for CO_2 geological sequestration. Journal of Petroleum Science and Engineering, 78, 765-777.

Yamamoto, H. and Doughty, C., 2011, Investigation of gridding effects for numerical simulations of CO_2 geologic sequestration. International Journal of Greenhouse Gas Control, 5, 975-985.

Yeh, G.T., 2000, Computational subsurface hydrology: Reactions, transport, and fate. Kluwer Academic Publishers, Boston, Massachusetts, USA.

Zhang, W., Li, Y., Xu, T., Cheng, H., Zheng, Y. and Xiong, P., 2009, Long-term variations of CO_2 trapped in different mechanisms in deep saline

formations: A case study of the Songliao Basin, China. International Journal of Greenhouse Gas Control, 3, 161-180.

Zhang, K., Wu, Y.S. and Pruess, K., 2008, User's guide for TOUGH2-MP - A massively parallel version of the TOUGH2 code. Technical Report LBNL-315E, Lawrence Berkeley National Laboratory, University of California, Berkeley, California, USA, 108 p.

국문 초록 (Abstract in Korean)

심부 저장 지층에 주입된 이산화탄소의 거동 및 포획에 대한 격자 세분할 영향을 정량적으로 평가하기 위하여 일련의 다상 유체 열–수리학적 수치 모델링을 수행하였다. 먼저 가상의 삼차원 저장 지층을 이산화하여 하나의 대표 경우 격자를 만들고 이를 다시 수직, 수평, 수직 · 수평 방향으로 2 배, 4 배, 8 배로 세분할 하였다. 수치 모델링 결과는 이산화탄소 거동(자유 유체상 및 수용액 상) 및 포획 기작(수리동력학적 포획 및 용해 포획)은 수직(z), 수평(xy), 수직 · 수평(xyz) 방향으로 격자 세분할에 시공간적으로 크게 영향을 받음을 보여준다. 이는 수직, 수평, 수직 · 수평 방향으로 격자 세분할이 주입된 이산화탄소와 주변 지하수 사이의 가파른 절단면(sharp fronts)을 정밀하게 고려하고 저장 지층의 압력 및 온도를 정밀하게 반영하기 때문이다. 그 결과 격자 세분할 방향에 관계없이 주입 기간 동안 상대적으로 성근 격자는 시공간적으로 넓은 지역에 걸쳐 완만한 전단면(smooth fronts)을 가진다. 마찬가지로 주입 종료 이후 상대적으로 성근 격자는 넓은 지역에 걸쳐 완만한 전단면을 가지며 수평 방향의 영향 반경을 과소평가한다. 한편 격자 세분할

방향과 무관하게 이산화탄소는 주입 기간 동안 주로 수평 방향으로 이동하고 이산화탄소는 주입 종료 이후 주로 수직 방향으로 이동한다. 그 결과 수평 방향으로 격자 세분할은 주로 주입 기간 동안 이산화탄소의 거동 및 포획에 영향을 크게 미치고 반면에 수직 방향으로 격자 세분할은 주로 주입 종료 이후 이산화탄소의 거동 및 포획에 영향을 크게 미친다. 그러므로 수직 · 수평 방향으로 격자 세분할의 결과는 주입 기간 동안 시공간적으로 이산화탄소의 거동과 포획 기작 효율이 수평 방향으로 격자 세분할 결과와 유사함을 보여주고 주입 종료 이후는 수직 방향으로 격자 세분할 결과와 유사함을 보여준다. 따라서 이산화탄소 지중 저장에 의한 거동 및 포획 기작을 주입 기간뿐만 아니라 주입 이후에도 정밀하게 분석하고 평가하기 위해서는 수직 · 수평 방향으로 모두 격자를 고려하는 것이 합당하다.

주요어: 이산화탄소 지중 저장, 심부 저장 지층, 거동 기작, 포획 기작, 격자 세분할, 수치 모델링

학 번: 2013-20336